μ-diff: an open-source Matlab toolbox for computing multiple scattering problems by disks

Bertrand Thierry, Xavier Antoine, Chokri Chniti, Hasan Alzubaidi

μ-diff: an open-source Matlab toolbox for computing multiple scattering problems by disks

Bertrand Thierry*[1], Xavier Antoine†[2], Chokri Chniti‡[3], and Hasan Alzubaidi§[4]

[1]Laboratoire J.L. Lions (LJLL), University of Paris VI, Paris, France.
[2]Université de Lorraine, Institut Elie Cartan de Lorraine, UMR 7502, Vandoeuvre-lès-Nancy, F-54506, France.
[3]Department of Mathematics, University College in Qunfudah, Umm Al-Qura University, Saudi Arabia.

Abstract

The aim of this paper is to describe a Matlab toolbox, called μ-diff, for modeling and numerically solving two-dimensional complex multiple scattering by a large collection of circular cylinders. The approximation methods in μ-diff are based on the Fourier series expansions of the four basic integral operators arising in scattering theory. Based on these expressions, an efficient spectrally accurate finite-dimensional solution of multiple scattering problems can be simply obtained for complex media even when many scatterers are considered as well as large frequencies. The solution of the global linear system to solve can use either direct solvers or preconditioned iterative Krylov subspace solvers for block Toeplitz matrices. Based on this approach, this paper explains how the code is built and organized. Some complete numerical examples of applications (direct and inverse scattering) are provided to show that μ-diff is a flexible, efficient and robust toolbox for solving some complex multiple scattering problems.

Keywords: Multiple scattering, wave propagation, acoustics, electromagnetism, optics, computational methods, numerical simulation, spectral method

PACS: 02.60.-x, 02.70.-c, 31.15.-p, 31.15.xf

MSC: 35J05, 78A45, 78A48, 76Q05, 65M70, 31A10

Contents

*bthierry@math.cnrs.fr
†xavier.antoine@univ-lorraine.fr, corresponding author
‡cachniti@uqu.edu.sa
§hmzubaidi@uqu.edu.sa

1 Program Summary

Manuscript title: μ-diff: an open Matlab toolbox for computing multiple scattering problems by disks

Authors: Xavier ANTOINE & Bertrand THIERRY

Program title: μ-diff

Licensing provisions: Standard CPC licence

Programming language: Matlab

Computer(s) for which the program has been designed: PC, Mac

Operating system(s) for which the program has been designed: Windows, Mac OS, Linux

RAM required to execute with typical data: 2000 Megabytes

Has the code been vectorised or parallelized?: Yes

Number of processors used: Most if not all

Keywords: Matlab, Multiple scattering, waves, random media, acoustics, optics, electromagnetism, numerical methods

CPC Library Classification: 4.6, 10, 18

Nature of problem: Modeling and simulation of two-dimensional multiple wave scattering by large clusters of circular cylinders for any frequency. The program is well-designed to manage highly accurate solutions for deterministic or random media, with various boundary conditions and physics properties of the scatterers. Pre- and post-processing facilities are designed specifically for these problems.

Solution method: We use spectral Fourier approximation schemes and direct or iterative Krylov subspace methods.
Running time: From a few seconds for simple problems to a few minutes for more complex situations on a medium computer.

2 Introduction

Let us consider M regular, bounded and disjoint scatterers Ω_p^-, $p = 1, ..., M$, distributed in $\mathbb{R}^2$, with boundary $\Gamma_p := \partial\Omega_p^-$. The scatterer Ω^- is defined as the collection of the M separate obstacles, i.e. $\Omega^- = \cup_{p=1}^M \Omega_p^-$, with boundary $\Gamma = \cup_{p=1}^M \Gamma_p$. The homogeneous and isotropic exterior domain of propagation is $\Omega^+ = \mathbb{R}^2 \setminus \overline{\Omega^-}$. For the sake of conciseness in the presentation, we first assume that the scatterers are sound-soft (Dirichlet boundary condition), but other situations can be handled by the μ-diff (**mu**ltiple-**diff**raction) Matlab toolbox (e.g. sound-hard scatterers, impedance boundary conditions, penetrable scatterers) as it will be shown during the numerical examples (see section 7). We now consider a time-harmonic incident acoustic plane wave $u^{\text{inc}}(\mathbf{x}) = e^{-ik\boldsymbol{\beta}\cdot\mathbf{x}}$ (with $\mathbf{x} = (x_1, x_2) \in \mathbb{R}^2$) illuminating Ω^-, with an incidence direction $\boldsymbol{\beta} = (\cos(\beta), \sin(\beta))$ and a time dependence $e^{-i\omega t}$, where ω is the wave pulsation and $k = 2\pi/\lambda$ is the wavenumber, λ being the wavelength. The sound-soft multiple scattering problem of u^{inc} by Ω^- consists in computing the scattered wavefield u as the solution to the boundary-value problem [7, 37]

$$\left\{\begin{array}{rcll} (\Delta + k^2)u & = & 0, & \text{in } \Omega^+, \\ u & = & -u^{\text{inc}}, & \text{on } \Gamma, \\ \lim\limits_{||\mathbf{x}||\to+\infty} ||\mathbf{x}||^{1/2} \left(\nabla u \cdot \dfrac{\mathbf{x}}{||\mathbf{x}||} - iku\right) & = & 0. & \end{array}\right. \tag{1}$$

The operator $\Delta = \partial_{x_1}^2 + \partial_{x_2}^2$ is the Laplace operator and $(\Delta + k^2)$ is the Helmholtz operator. The gradient operator is ∇ and $||\mathbf{x}|| = \sqrt{\mathbf{x}\cdot\mathbf{x}}$, where $\mathbf{x}\cdot\mathbf{y}$ is the scalar product of two vectors $\mathbf{x}$ and $\mathbf{y}$ of $\mathbb{R}^2$. The last equation of (1) is the well-known Sommerfeld's radiation condition at infinity that ensures the uniqueness of u [18, 41].

Multiple scattering is known to be a very complicated and challenging problem in terms of computational method [1, 2, 3, 7, 8, 16, 22, 23, 28, 30, 36, 52] since the incident wave is multiply diffracted by all the single scatterers involved in the geometrical configuration. As a consequence, the scattered wavefield has a highly complicated structure and exhibits some particular physics properties. The toolbox μ-diff* contributes to the development of reliable and efficient numerical methods to understand and simulate such problems. It uses the powerful and mathematically rigorous integral equation formulation methods for solving multiple scattering problems. Being able to use integral operators allows us to formulate the solution to a given scattering problem by using traces theorems and variational approaches (see section 3). When the boundary Γ is general, then boundary element discretization techniques are required [6, 7, 18, 37, 41, 45]. Even if these methods are extremely useful for general shapes, they also have some disadvantages. First, they lead to solving large full linear systems, most particularly when investigating small wavelength problems ($\lambda \ll 1$) and large scatterers ($\text{size}(\Omega^-) \gg 1$) or collections of many scatterers ($M \gg 1$). These systems require a lot of memory storage and their solution is highly time consuming. The solution can be accelerated by using Krylov subspace solvers [4, 5, 6, 44] in conjunction with fast

*`http://mu-diff.math.cnrs.fr`

matrix-vector products algorithms (for example Multilevel Fast Multipole Methods [29] or other compression techniques [7, 28]) but at the price of a loss of accuracy/stability. Second, even if boundary element methods provide an accurate solution, the precision is limited when linear finite element spaces are used as well as low-order surface descriptions. Going to higher order basis functions is very complicated and time consuming, most particularly when one wants to integrate with high accuracy (hyper)singular potentials that are involved in an integral formulation.

When the geometry is more trivial, then further simplifications can be realized in the integral equation methods. Indeed, for example, analytical expressions of the integral operators can be obtained, and spectrally accurate and fast solutions can be derived. This is the case when considering a disk [7, 37]. The Matlab toolbox μ-diff considers the case of a collection of M homogeneous circular cylinders where Fourier basis expansions can be used (see section 4). Even if disks can be considered as simple geometries, a reliable and highly accurate solution is required for wave propagation problems (acoustics, electromagnetics, optics, nanophotonics, elasticity) that involve many circular scatterers, modeling structured or disordered media, most particularly when k and M are large (see e.g. [9, 15, 19, 20, 21, 22, 24, 33, 34, 35, 36, 39, 40, 42, 46, 50, 51, 53]). Let us note that all the developments in this paper directly apply to 2D transverse magnetic/electric electromagnetic scattering waves [37] even if our presentation is more related to acoustics. Furthermore, since multiple scattering is a highly complex problem with unusual properties, it is desirable to have a simple modeling tool that helps to understand the physics properties of such structures. Finally, having a reference solution method for multiple scattering leads to the possibility of evaluating the accuracy and performance of other more general numerical methods like finite element or general integral equation solvers. The goal of the μ-diff Matlab toolbox is to contribute to these different questions.

The structure of the paper is the following. In section 3, we describe the basics of integral operators that are used in μ-diff and review the most standard integral equation formulations when one wants to solve the sound-soft scattering problem. In Section 4, we explain the approximation method that is used in μ-diff to solve the integral equation problems through Fourier series expansions and how to formulate post-processing data (near- and far-fields for example). In section 5, we describe the finite-dimensional approximation leading to concrete linear systems. Some numerical aspects of the resolution methods are also discussed. Section 6 details the structure of the μ-diff code and the main functions that are included. To illustrate the use of μ-diff, we provide in sections 7.1 and 7.2 some numerical examples for direct multiple scattering problems (sound-soft, sound-hard, penetrable scatterers). In addition, we consider in section 7.3 a more advanced example related to the DORT method (Time Reversal method) in the presence of homogeneous penetrable circular scatterers. All the related files are available in the μ-diff package when downloaded and the simulations can be reproduced. Finally, we conclude in section 8.

3 Basic theory behind μ-diff: integral equations and formulations for 2D scattering problems

3.1 Definitions and basics on integral operators for scattering

Let G be the two-dimensional free-space Green's function defined by

$$\forall \mathbf{x}, \mathbf{y} \in \mathbb{R}^2, \mathbf{x} \neq \mathbf{y}, \quad G(\mathbf{x}, \mathbf{y}) = \frac{i}{4} H_0^{(1)}(k\|\mathbf{x} - \mathbf{y}\|).$$

The function $H_0^{(1)}$ is the first-kind Hankel function of order zero. Integral equations are essentially based upon the Helmholtz integral representation formula [18, Theorems 3.1 and 3.3].

Proposition 1. *If v is a solution to the Helmholtz equation in the unbounded connected domain Ω^+ and satisfies the Sommerfeld radiation condition, then we have*

$$\int_\Gamma -G(\mathbf{x},\mathbf{y})\partial_{\mathbf{n}}v(\mathbf{y}) + \partial_{\mathbf{n_y}}G(\mathbf{x},\mathbf{y})v(\mathbf{y})\,\mathrm{d}\Gamma(\mathbf{y}) = \begin{cases} v(\mathbf{x}) & \text{if } \mathbf{x}\in\Omega^+, \\ 0 & \text{otherwise.} \end{cases} \tag{2}$$

If v^- is solution to the Helmholtz equation in the bounded domain Ω^-, then one gets

$$\int_\Gamma -G(\mathbf{x},\mathbf{y})\partial_{\mathbf{n}}v^-(\mathbf{y}) + \partial_{\mathbf{n_y}}G(\mathbf{x},\mathbf{y})v^-(\mathbf{y})\,\mathrm{d}\Gamma(\mathbf{y}) = \begin{cases} 0 & \text{if } \mathbf{x}\in\Omega^+, \\ -v^-(\mathbf{x}) & \text{otherwise.} \end{cases} \tag{3}$$

The unit normal vector $\mathbf{n}$ is outwardly directed to Ω^-. The integrals on Γ must be understood as duality brackets between the Sobolev space $H^{1/2}(\Gamma)$ and its dual space $H^{-1/2}(\Gamma)$. Nevertheless, when the incident wavefield u^{inc} and the curve Γ are sufficiently smooth, the scattered field is then regular and the duality bracket can be identified (this is systematically the case in the presentation) to the (non-Hermitian) inner product in $L^2(\Gamma)$

$$\langle f, g\rangle_{H^{-1/2},H^{1/2}} = \int_\Gamma f g d\Gamma.$$

Let us now introduce the volume single- and double-layer integral operators, respectively denoted by $\mathscr{L}$ and $\mathscr{M}$, and defined by: $\forall \mathbf{x}\in\mathbb{R}^2\backslash\Gamma$

$$\begin{aligned} \mathscr{L} : \rho &\longmapsto \mathscr{L}\rho(\mathbf{x}) = \int_\Gamma G(\mathbf{x},\mathbf{y})\rho(\mathbf{y})\,\mathrm{d}\Gamma(\mathbf{y}), \\ \mathscr{M} : \lambda &\longmapsto \mathscr{M}\lambda(\mathbf{x}) = -\int_\Gamma \partial_{\mathbf{n_y}}G(\mathbf{x},\mathbf{y})\lambda(\mathbf{y})\,\mathrm{d}\Gamma(\mathbf{y}). \end{aligned}$$

We can then express the wavefields v and v^- (see equations 2 and 3) as

$$\begin{cases} v(\mathbf{x}) = -\mathscr{L}(\partial_{\mathbf{n}}v|_\Gamma)(\mathbf{x}) - \mathscr{M}(v|_\Gamma)(\mathbf{x}), & \forall \mathbf{x}\in\Omega^+, \\ v^-(\mathbf{x}) = \mathscr{L}(\partial_{\mathbf{n}}v^-|_\Gamma)(\mathbf{x}) + \mathscr{M}(v^-|_\Gamma)(\mathbf{x}), & \forall \mathbf{x}\in\Omega^-. \end{cases}$$

Furthermore, the single- and double-layer integral operators provide some outgoing solutions to the Helmholtz equation [17].

Proposition 2. *For any densities $\rho\in H^{-1/2}(\Gamma)$ and $\lambda\in H^{1/2}(\Gamma)$, the functions $\mathscr{L}\rho$, $\mathscr{M}\lambda$ and any linear combination of them are some outgoing solutions to the Helmholtz equation in $\mathbb{R}^2\backslash\Gamma$ for some boundary conditions.*

We now recall the expressions of the trace and normal derivative trace of the volume single- and double-layer potentials which are commonly called jump relations [17, Theorem 3.1].

Proposition 3. *For any* $\mathbf{x}$ *in* Γ*, the trace and normal derivative traces of the operators* $\mathscr{L}$ *and* $\mathscr{M}$ *are given by the following relations (the signs indicate that* z *tends towards* x *from the exterior or the interior of* Γ*)*

$$\begin{aligned} &\lim_{\mathbf{z}\in\Omega^{\pm}\to\mathbf{x}} \mathscr{L}\rho(\mathbf{z}) = L\rho(\mathbf{x}), && \lim_{\mathbf{z}\in\Omega^{\pm}\to\mathbf{x}} \mathscr{M}\lambda(\mathbf{z}) = \left(\mp\frac{1}{2}I + M\right)\lambda(\mathbf{x}), \\ &\lim_{\mathbf{z}\in\Omega^{\pm}\to\mathbf{x}} \partial_{\mathbf{n_z}}\mathscr{L}\rho(\mathbf{z}) = \left(\mp\frac{1}{2}I + N\right)\rho(\mathbf{x}), && \lim_{\mathbf{z}\in\Omega^{\pm}\to\mathbf{x}} \partial_{\mathbf{n_z}}\mathscr{M}\lambda(\mathbf{z}) = D\lambda(\mathbf{x}), \end{aligned} \tag{4}$$

where I *is the identity operator, for* $\mathbf{x}\in\Gamma$*,*

$$\begin{aligned} &L\rho(\mathbf{x}) = \int_\Gamma G(\mathbf{x},\mathbf{y})\rho(\mathbf{y})\mathrm{d}\Gamma(\mathbf{y}), && M\lambda(\mathbf{x}) = -\int_\Gamma \partial_{\mathbf{n_y}}G(\mathbf{x},\mathbf{y})\lambda(\mathbf{y})\mathrm{d}\Gamma(\mathbf{y}), \\ &N\rho(\mathbf{x}) = \int_\Gamma \partial_{\mathbf{n_x}}G(\mathbf{x},\mathbf{y})\rho(\mathbf{y})\mathrm{d}\Gamma(\mathbf{y}) = -M^*\rho(\mathbf{x}), && D\lambda(\mathbf{x}) = -\partial_{\mathbf{n_x}}\int_\Gamma \partial_{\mathbf{n_y}}G(\mathbf{x},\mathbf{y})\lambda(\mathbf{y})\mathrm{d}\Gamma(\mathbf{y}). \end{aligned}$$

Throughout the paper, the boundary integral operators are denoted by a roman letter (e.g. L) while the volume integral operators use a calligraphic letter (e.g. $\mathscr{L}$). The operator $M^* = -N$ is the adjoint operator of M, that is

$$\langle g, Mf\rangle_{H^{-1/2},H^{1/2}} = \langle -Ng, f\rangle_{H^{-1/2},H^{1/2}}, \qquad \forall (f,g)\in H^{1/2}(\Gamma)\times H^{-1/2}(\Gamma).$$

Other properties like compactness or invertibility of integral operators can also be stated [7, 18, 41].

3.2 A few boundary integral equations for the Dirichlet problem

The aim of this section is to provide without details the most standard integral equation formulations for solving the 2D scattering problem with Dirichlet boundary condition. These equations serve as model examples for explaining the way μ-diff works in sections 6 and 7. We refer to [6, 47, 48] for further explanations concerning the derivation and properties of these integral equations (like for the well-posedness and the possible existence of resonant modes).

The first three integral equations presented here are based on a single-layer representation only

$$u = \mathscr{L}\rho. \tag{5}$$

From this representation and by using the jump relations, it can be proved that the density ρ is equal to $(-\partial_{\mathbf{n}}u - \partial_{\mathbf{n}}u^{\mathrm{inc}})|_\Gamma$ and thus has a physical meaning. The first integral equation, which is usually called Electric Field Integral Equation (EFIE), is based on the trace of the single-layer operator

$$L\rho = -u^{\mathrm{inc}}|_\Gamma. \tag{6}$$

The equation is well-posed and equivalent to the exterior scattering problem (1) as soon as k is not an irregular interior frequency of the associated Dirichlet boundary-value problem [6, 47].

A second equation, designated by Magnetic Field Integral Equation (MFIE), is

$$\left(\frac{1}{2}I + N\right)\rho = -\partial_{\mathbf{n}}u^{\mathrm{inc}}|_\Gamma.$$

It is also well-posed and equivalent to the exterior scattering problem (1) if k is not an interior Neumann resonance [6, 47]. Let us remark here that once ρ has been computed, the integral

equation (5) is again used for computing the exterior wavefield, and, in particular, the far-field (RCS).

To avoid the interior resonance problem, Burton and Miller [6, 14, 47] consider a linear combination of the EFIE and MFIE. Let α be a real-valued parameter such that: $0 < \alpha < 1$, and η be a complex number which satisfies $\Im(\eta) \neq 0$, where $\Im(\eta)$ is the imaginary part of η (the real part is $\Re(\eta)$). Then, the Combined Field Integral Equation (CFIE) [6, 31, 47] (also called Burton-Miller integral equation) is given by

$$\left[(1-\alpha)\left(\frac{1}{2}I + N\right) + \alpha\eta L\right]\rho = -\left[(1-\alpha)\partial_{\mathbf{n}}u^{\text{inc}}|_{\Gamma} + \alpha\eta u^{\text{inc}}|_{\Gamma}\right].$$

This integral equation is well-posed for any wavenumber k. Again, the exterior field can be obtained thanks to the integral equation (5).

Let us now consider η as a complex-valued parameter with non zero imaginary part. Then, a fourth integral representation is based on a linear combination of the single- and double-layer potentials

$$u^{\text{tot}} = -(\eta\mathscr{L} + \mathscr{M})\psi + u^{\text{inc}},$$

where the total wavefield is defined by $u^{\text{tot}} := u + u^{\text{inc}}$. The resulting integral equation is obtained by taking the trace of the above relation (see equations (4))

$$\left[-\eta L - M + \frac{1}{2}I\right]\psi = -u^{\text{inc}}|_{\Gamma}. \tag{7}$$

This equation, called Brakhage-Werner Integral Equation (BWIE) [12], is well-posed for any k and is equivalent to the exterior scattering problem. Finally, let us note that the surface density ψ is unphysical unlike for the three previous equations.

When $\Omega^- = \bigcup_{p=1}^{M}\Omega_p^-$ is assumed to be multiply connected, all the integral operators can be written by blocks. For example, the single-layer potential $\mathscr{L}\rho$ can be expressed as the sum of elementary potentials

$$\mathscr{L}\rho = \sum_{p=1}^{M}\mathscr{L}_p\rho_p,$$

where $\rho_p = \rho|_{\Gamma_p}$ and

$$\mathscr{L}_p\rho_p(\mathbf{x}) = \int_{\Gamma_p} G(\mathbf{x},\mathbf{y})\rho_p(\mathbf{y})\,\mathrm{d}\mathbf{x}, \qquad \forall\mathbf{x}\in\mathbb{R}^2\backslash\overline{\Omega_p^-}.$$

Another way of writing the EFIE (6) is then

$$\begin{pmatrix} L_{1,1} & L_{1,2} & \dots & L_{1,M} \\ L_{2,1} & L_{2,2} & \dots & L_{2,M} \\ \vdots & \vdots & \ddots & \vdots \\ L_{M,1} & L_{M,2} & \dots & L_{M,M} \end{pmatrix}\begin{pmatrix} \rho_1 \\ \rho_2 \\ \vdots \\ \rho_M \end{pmatrix} = -\begin{pmatrix} u^{\text{inc}}|_{\Gamma_1} \\ u^{\text{inc}}|_{\Gamma_2} \\ \vdots \\ u^{\text{inc}}|_{\Gamma_M} \end{pmatrix},$$

where $L_{p,q}\rho_q = (L_q\rho_q)|_{\Gamma_p}$, with

$$\forall\mathbf{x}\in\Gamma, L_q\rho_q(\mathbf{x}) = \int_{\Gamma_q} G(\mathbf{x},\mathbf{y})\rho_q(\mathbf{x})\,\mathrm{d}\mathbf{y}.$$

In the same way, the three other operators N, M and D can be written in terms of elementary operators $N_{p,q}$, $M_{p,q}$ and $D_{p,q}$.

4 Spectral formulation used in μ-diff

We consider now circular cylinders as scatterers. In this situation, we can explicitly compute the boundary integral equations in a Fourier basis, leading therefore to an efficient computational spectral method when used in conjunction with numerical linear algebra methods (direct or iterative solvers).

4.1 Notations and Fourier basis

Let us consider an orthonormal system $(\mathbf{O}, \overrightarrow{\mathbf{O}x_1}, \overrightarrow{\mathbf{O}x_2})$. We assume that the scattering obstacle Ω^- is the union of M disks Ω_p^-, for $p = 1, \ldots, M$, of radius a_p and center $\mathbf{O}_p$. We define Γ_p as the boundary of Ω_p^- and by $\Gamma = \cup_{p=1\ldots M}\Gamma_p$ the boundary of Ω^-. The unit normal vector $\mathbf{n}$ to Ω^- is outgoing. An illustration of the notations is reported on Figure 1.

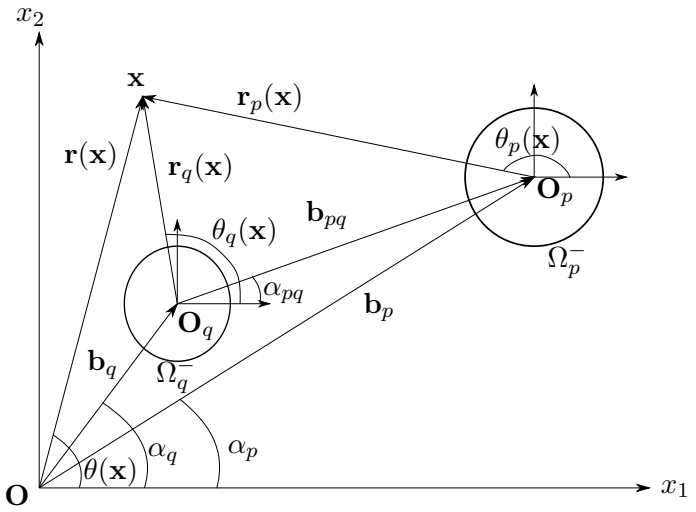

Figure 1: Illustration of the notations for two disks Ω_p^- and Ω_q^- and a point $\mathbf{x} \in \Omega^+$.

For any $p = 1, \ldots, M$, we introduce $\mathbf{b}_p$ as the vector between the center $\mathbf{O}_p$ and the origin $\mathbf{O}$

$$\mathbf{b}_p = \mathbf{O}\mathbf{O}_p, \qquad b_p = \|\mathbf{b}_p\|, \qquad \alpha_p = Angle(\overrightarrow{\mathbf{O}x_1}, \mathbf{b}_p),$$

and, for $q = 1, \ldots, M$, with $q \neq p$, $\mathbf{b}_{pq}$ as the vector between the centers $\mathbf{O}_q$ and $\mathbf{O}_p$

$$\mathbf{b}_{pq} = \mathbf{O}_q\mathbf{O}_p, \qquad b_{pq} = \|\mathbf{b}_{pq}\|, \qquad \alpha_{pq} = Angle(\overrightarrow{\mathbf{O}x_1}, \mathbf{b}_{pq}).$$

Furthermore, any point $\mathbf{x}$ is described by its global polar coordinates

$$\mathbf{r}(\mathbf{x}) = \mathbf{O}\mathbf{x}, \qquad r(\mathbf{x}) = \|\mathbf{r}(\mathbf{x})\|, \qquad \theta(\mathbf{x}) = Angle(\overrightarrow{\mathbf{O}x_1}, \mathbf{r}(\mathbf{x})),$$

or by its polar coordinates in the orthonormal system associated with the obstacle Ω_p^-, with $p = 1, \ldots, M$,

$$\mathbf{r}_p(\mathbf{x}) = \mathbf{O}_p\mathbf{x}, \qquad r_p(\mathbf{x}) = \|\mathbf{r}_p(\mathbf{x})\|, \qquad \theta_p(\mathbf{x}) = Angle(\overrightarrow{\mathbf{O}_p x_1}, \mathbf{r}_p(\mathbf{x})).$$

Let us now build a basis of $L^2(\Gamma)$ to approximate the integral operators. To this end, we first construct a basis of $L^2(\Gamma_p)$ associated with Ω_p^-, for $p = 1, \ldots, M$. If the circle Γ_p has a radius one and is centered at the origin, then a suitable basis of $L^2(\Gamma_p)$ is the spectral Fourier basis of functions $(e^{im\theta})_{m\in\mathbb{Z}}$. We adapt this basis to the general case where $a_p \neq 1$ by introducing, on one hand, the functions $(\varphi_m)_{m\in\mathbb{Z}}$ defined on $\mathbb{R}^2$ by: $\forall m \in \mathbb{Z}$, $\forall \mathbf{x} \in \mathbb{R}^2$, $\varphi_m(\mathbf{x}) = e^{im\theta(\mathbf{x})}$, and, on the other hand, the functions $(\varphi_m^p)_{1\leqslant p\leqslant M,\, m\in\mathbb{Z}}$ given by

$$\forall p = 1, \ldots, M, \forall m \in \mathbb{Z}, \forall \mathbf{x} \in \Gamma_p, \qquad \varphi_m^p(\mathbf{x}) = \frac{\varphi_m(\mathbf{r}_p(\mathbf{x}))}{\sqrt{2\pi a_p}} = \frac{e^{im\theta_p(\mathbf{x})}}{\sqrt{2\pi a_p}}.$$

For $p = 1, \ldots, M$, the family $(\varphi_m^p)_{m\in\mathbb{Z}}$ forms an orthonormal basis of $L^2(\Gamma_p)$ for the Hermitian inner product $(\cdot,\cdot)_{L^2(\Gamma_p)}$

$$\forall f, g \in L^2(\Gamma_p), \qquad (f,g)_{L^2(\Gamma_p)} = \int_{\Gamma_p} f(\mathbf{x})\overline{g(\mathbf{x})}\mathrm{d}\Gamma_p(\mathbf{x}).$$

To build a basis of $L^2(\Gamma)$, we introduce the functions Φ_m^p of $L^2(\Gamma)$ as the union of these M families

$$\forall p, q = 1, \ldots, M, \forall m \in \mathbb{Z}, \qquad \Phi_m^p|_{\Gamma_q} = \begin{cases} 0 & \text{if } q \neq p, \\ \varphi_m^p & \text{if } q = p. \end{cases}$$

The family $\mathscr{B} = \{\Phi_m^p,\, m \in \mathbb{Z}, p = 1, \ldots, M\}$, also called Fourier or spectral basis, is a Hilbert basis of $L^2(\Gamma)$ for the usual scalar product $(\cdot,\cdot)_{L^2(\Gamma)}$.

4.2 Integral operators - integral equations for a cluster of circular cylinders

In view of a numerical procedure, μ-diff uses the weak formulation of the EFIE (6) in $L^2(\Gamma)$ based on the Fourier basis $\mathscr{B}$

$$\begin{cases} \text{Find } \rho \in H^{-1/2}(\Gamma) \text{ such that for any } p = 1, \ldots, M, \text{ and } m \in \mathbb{Z}, \\ (L\rho, \Phi_m^p)_{L^2(\Gamma)} = -\left(u^{\mathrm{inc}}|_\Gamma, \Phi_m^p\right)_{L^2(\Gamma)}. \end{cases}$$

Since u^{inc} is assumed to be smooth enough (typically $\mathscr{C}^\infty$) and that Γ is $\mathscr{C}^\infty$, then the scattered wavefield is also $\mathscr{C}^\infty(\Omega^+)$ and the density ρ is (at least) in $H^{1/2}(\Gamma)$. Therefore, ρ can be expanded in $\mathscr{B}$ as

$$\rho = \sum_{q=1}^{M} \sum_{n\in\mathbb{Z}} \rho_n^q \Phi_n^q$$

and the weak form of the EFIE is

$$\begin{cases} \text{Find the Fourier coefficients } \rho_n^q \in \mathbb{C}, \text{ for } q = 1, \ldots, M, \text{ and } n \in \mathbb{Z}, \text{ such that,} \\ \forall p = 1, \ldots, M,\ \forall m \in \mathbb{Z}, \qquad \displaystyle\sum_{q=1}^{M} \sum_{n\in\mathbb{Z}} \rho_n^q \left(L\Phi_n^q, \Phi_m^p\right)_{L^2(\Gamma)} = -\left(u^{\mathrm{inc}}|_\Gamma, \Phi_m^p\right)_{L^2(\Gamma)}. \end{cases}$$

This formulation can be written under the following matrix form $\widetilde{\mathbb{L}}\widetilde{\boldsymbol{\rho}} = \widetilde{\mathbf{U}}$, where the infinite matrix representation $\widetilde{\mathbb{L}} = (\widetilde{\mathbb{L}}^{p,q})_{1\leqslant p,q\leqslant M}$ and the infinite vectors $\widetilde{\boldsymbol{\rho}} = (\widetilde{\boldsymbol{\rho}}^p)_{1\leqslant p\leqslant M}$ and $\widetilde{\mathbf{U}} = (\widetilde{\mathbf{U}}^p)_{1\leqslant p\leqslant M}$ are

defined by blocks as

$$\widetilde{\mathbb{L}} = \begin{bmatrix} \widetilde{\mathbb{L}}^{1,1} & \widetilde{\mathbb{L}}^{1,2} & \dots & \widetilde{\mathbb{L}}^{1,M} \\ \widetilde{\mathbb{L}}^{2,1} & \widetilde{\mathbb{L}}^{2,2} & \dots & \widetilde{\mathbb{L}}^{2,M} \\ \vdots & \vdots & \ddots & \vdots \\ \widetilde{\mathbb{L}}^{M,1} & \widetilde{\mathbb{L}}^{M,2} & \dots & \widetilde{\mathbb{L}}^{M,M} \end{bmatrix}, \qquad \widetilde{\boldsymbol{\rho}} = \begin{bmatrix} \widetilde{\boldsymbol{\rho}}^1 \\ \widetilde{\boldsymbol{\rho}}^2 \\ \vdots \\ \widetilde{\boldsymbol{\rho}}^M \end{bmatrix}, \qquad \widetilde{\mathbf{U}} = \begin{bmatrix} \widetilde{\mathbf{U}}^1 \\ \widetilde{\mathbf{U}}^2 \\ \vdots \\ \widetilde{\mathbf{U}}^M \end{bmatrix}, \tag{8}$$

with, for any $p, q = 1, \dots, M$, and $m, n \in \mathbb{Z}$: $\widetilde{\mathbb{L}}^{p,q}_{m,n} = (L\Phi^q_n, \Phi^p_m)_{L^2(\Gamma)}$, $\widetilde{\boldsymbol{\rho}}^p_m = \rho^p_m$ and $\widetilde{\mathbf{U}}^p_m = \left(-u^{\mathrm{inc}}|_\Gamma, \Phi^p_m\right)_{L^2(\Gamma)}$.

For the other integral formulations (section 3.2) or even for any other boundary condition, the expressions of the three boundary integral operators M, N and D are needed. Therefore, to compute an integral equation, we introduce the infinite matrices $\widetilde{\mathbb{M}} = (\widetilde{\mathbb{M}}^{p,q})_{1\leqslant p,q\leqslant M}$, $\widetilde{\mathbb{N}} = (\widetilde{\mathbb{N}}^{p,q})_{1\leqslant p,q\leqslant M}$ and $\widetilde{\mathbb{D}} = (\widetilde{\mathbb{D}}^{p,q})_{1\leqslant p,q\leqslant M}$, with the same block structure as $\widetilde{\mathbb{L}}$ (see equation (8)). For $p, q = 1, \dots, M$, the coefficients of the infinite matrices $\widetilde{\mathbb{M}}^{p,q}$, $\widetilde{\mathbb{N}}^{p,q}$ and $\widetilde{\mathbb{D}}^{p,q}$ are defined for any indices m and n in $\mathbb{Z}$ by

$$\widetilde{\mathbb{M}}^{p,q}_{m,n} = (M\Phi^q_n, \Phi^p_m)_{L^2(\Gamma)}, \widetilde{\mathbb{N}}^{p,q}_{m,n} = (N\Phi^q_n, \Phi^p_m)_{L^2(\Gamma)}, \text{ and } \widetilde{\mathbb{D}}^{p,q}_{m,n} = (D\Phi^q_n, \Phi^p_m)_{L^2(\Gamma)}.$$

For a numerical implementation, we can explicitly compute [8, 47] the matrix blocks $\widetilde{\mathbb{L}}^{p,q}$, $\widetilde{\mathbb{M}}^{p,q}$, $\widetilde{\mathbb{N}}^{p,q}$ and $\widetilde{\mathbb{D}}^{p,q}$ involved in $\widetilde{\mathbb{L}}$, $\widetilde{\mathbb{M}}$, $\widetilde{\mathbb{N}}$ and $\widetilde{\mathbb{D}}$, for $p, q = 1, \dots, M$. To this end, we introduce the infinite diagonal matrices $\widetilde{\mathbb{J}}^p$, $(\mathrm{d}\widetilde{\mathbb{J}})^p$, $\widetilde{\mathbb{H}}^p$ and $(\mathrm{d}\widetilde{\mathbb{H}})^p$, with general terms, for $m \in \mathbb{Z}$,

$$\widetilde{\mathbb{J}}^p_{mm} = J_m(ka_p), \quad (\mathrm{d}\widetilde{\mathbb{J}})^p_{mm} = J'_m(ka_p), \quad \widetilde{\mathbb{H}}^p_{mm} = H^{(1)}_m(ka_p), \quad (\mathrm{d}\widetilde{\mathbb{H}})^p_{mm} = H^{(1)'}_m(ka_p).$$

In addition, let $\widetilde{\mathbb{I}}^p$ be the infinite identity matrix, and, for $q \neq p$, the infinite separation matrix $\widetilde{\mathbb{S}}^{p,q}$ between the obstacles Ω^-_p and Ω^-_q, defined by

$$\widetilde{\mathbb{S}}^{p,q} = (\widetilde{\mathbb{S}}^{p,q}_{m,n})_{m\in\mathbb{Z},n\in\mathbb{Z}} \qquad \text{and} \qquad \widetilde{\mathbb{S}}^{p,q}_{m,n} = S_{mn}(\mathbf{b}_{pq}) = H^{(1)}_{m-n}(kb_{pq})e^{i(m-n)\alpha_{b_q}}.$$

Under these notations, we rewrite the blocks $\widetilde{\mathbb{L}}^{p,q}$, $\widetilde{\mathbb{M}}^{p,q}$, $\widetilde{\mathbb{N}}^{p,q}$ and $\widetilde{\mathbb{D}}^{p,q}$ of the infinite matrices $\widetilde{\mathbb{L}}$, $\widetilde{\mathbb{M}}$, $\widetilde{\mathbb{N}}$ and $\widetilde{\mathbb{D}}$ under the matrix form, for any $p, q = 1, \dots, M$,

- $\widetilde{\mathbb{L}}^{p,q} = \begin{cases} \dfrac{i\pi a_p}{2}\widetilde{\mathbb{J}}^p\widetilde{\mathbb{H}}^p, & \text{if } p = q, \\ \dfrac{i\pi\sqrt{a_pa_q}}{2}\widetilde{\mathbb{J}}^p(\widetilde{\mathbb{S}}^{p,q})^T\widetilde{\mathbb{J}}^q, & \text{if } p \neq q, \end{cases}$

- $\widetilde{\mathbb{M}}^{p,q} = \begin{cases} -\dfrac{1}{2}\widetilde{\mathbb{I}}^p - \dfrac{i\pi ka_p}{2}\widetilde{\mathbb{J}}^p(\mathrm{d}\widetilde{\mathbb{H}})^p = \dfrac{1}{2}\widetilde{\mathbb{I}}^p - \dfrac{i\pi ka_p}{2}(\mathrm{d}\widetilde{\mathbb{J}})^p\widetilde{\mathbb{H}}^p, & \text{if } p = q, \\ -\dfrac{ik\pi\sqrt{a_pa_q}}{2}\widetilde{\mathbb{J}}^p(\widetilde{\mathbb{S}}^{p,q})^T(\mathrm{d}\widetilde{\mathbb{J}})^q, & \text{if } p \neq q, \end{cases}$

- $\widetilde{\mathbb{N}}^{p,q} = \begin{cases} \dfrac{1}{2}\widetilde{\mathbb{I}}^p + \dfrac{i\pi ka_p}{2}\widetilde{\mathbb{J}}^p(\mathrm{d}\widetilde{\mathbb{H}})^p = -\dfrac{1}{2}\widetilde{\mathbb{I}}^p + \dfrac{i\pi ka_p}{2}(\mathrm{d}\widetilde{\mathbb{J}})^p\widetilde{\mathbb{H}}^p, & \text{if } p = q, \\ \dfrac{ik\pi\sqrt{a_pa_q}}{2}(\mathrm{d}\widetilde{\mathbb{J}})^p(\widetilde{\mathbb{S}}^{p,q})^T\widetilde{\mathbb{J}}^q, & \text{if } p \neq q, \end{cases}$

- $\widetilde{\mathbb{D}}^{p,q} = \begin{cases} \dfrac{i\pi k^2 a_p}{2}(\mathrm{d}\widetilde{\mathbb{J}})^p(\mathrm{d}\widetilde{\mathbb{H}})^p, & \text{if } p = q, \\ -\dfrac{ik^2\pi\sqrt{a_p a_q}}{2}(\mathrm{d}\widetilde{\mathbb{J}})^p(\widetilde{\mathbb{S}}^{p,q})^T(\mathrm{d}\widetilde{\mathbb{J}})^q, & \text{if } p \neq q, \end{cases}$

where $(\widetilde{\mathbb{S}}^{p,q})^T$ is the transpose matrix of the separation matrix $\widetilde{\mathbb{S}}^{p,q}$.

The integral equations involve the trace or normal derivative trace of the incident wavefield on Γ. We have already introduced the infinite vector $\widetilde{\mathbf{U}}$ of the coefficients of $u^{\mathrm{inc}}|_\Gamma$ in the Fourier basis. We then define similarly the infinite vector $\mathrm{d}\widetilde{\mathbf{U}} = (\mathrm{d}\widetilde{\mathbf{U}}^p)_{1\leqslant p\leqslant M}$ of the coefficients of the normal derivative trace $\partial_{\mathbf{n}} u^{\mathrm{inc}}|_\Gamma$, such that

$$\forall p = 1, \ldots, M,\ \forall m \in \mathbb{Z}, \qquad (\mathrm{d}\widetilde{\mathbf{U}})^p_m = \left(\partial_{\mathbf{n}} u^{\mathrm{inc}}|_\Gamma, \Phi^p_m\right)_{L^2(\Gamma)}.$$

Finally, the density changes according to the integral equation and most particularly with respect to the boundary condition. To keep the same notations as previously, we introduce the densities λ and ψ (used in the BWIE) that are expanded in the Fourier basis as

$$\lambda = \sum_{p=1}^{M}\sum_{m\in\mathbb{Z}} \lambda^p_m \Phi^p_m \qquad \text{and} \qquad \psi = \sum_{p=1}^{M}\sum_{m\in\mathbb{Z}} \psi^p_m \Phi^p_m.$$

Finally, we set: $\widetilde{\boldsymbol{\lambda}} = (\widetilde{\boldsymbol{\lambda}}^p)_{1\leqslant p\leqslant M}$ and $\widetilde{\Psi} = (\widetilde{\Psi}^p)_{1\leqslant p\leqslant M}$, where each block $\widetilde{\boldsymbol{\lambda}}^p = (\widetilde{\boldsymbol{\lambda}}^p_m)_{m\in\mathbb{Z}}$ and $\widetilde{\Psi}^p = (\widetilde{\Psi}^p_m)_{m\in\mathbb{Z}}$ is defined by: $\forall m \in \mathbb{Z}$, $\widetilde{\boldsymbol{\lambda}}^p_m = \lambda^p_m$ and $\widetilde{\Psi}^p_m = \psi^p_m$.

4.3 Projection of the incident waves in the Fourier basis

To fully solve one of the integral equations (EFIE, MFIE, CFIE or Brakhage-Werner), we need to compute the Fourier coefficients of the trace and normal derivative traces of the incident wave. We give the results for both an incident plane wave and a pointwise source term (Green's function).

For an incident plane wave, the following proposition holds [3].

Proposition 4. *Let us assume that u^{inc} is an incident plane wave of direction $\boldsymbol{\beta}$, with $\boldsymbol{\beta} = (\cos(\beta), \sin(\beta))$ and $\beta \in [0, 2\pi]$, i.e.*

$$\forall \mathbf{x} \in \mathbb{R}^2, \qquad u^{inc}(\mathbf{x}) = e^{-ik\boldsymbol{\beta}\cdot\mathbf{x}}.$$

Then we have the following equalities

$$\widetilde{\mathbf{U}}^p_m = \left(u^{inc}|_\Gamma, \Phi^p_m\right)_{L^2(\Gamma)} = d^p_m J_m(ka_p), \qquad (\mathrm{d}\widetilde{\mathbf{U}})^p_m = \left(\partial_{\mathbf{n}} u^{inc}|_\Gamma, \Phi^p_m\right)_{L^2(\Gamma)} = k d^p_m J'_m(ka_p),$$

with $d^p_m = \sqrt{2\pi a_p} e^{-ik\boldsymbol{\beta}\cdot\mathbf{b}_p} e^{im(\pi/2+\beta)}$.

Let us consider now an incident wave emitted by a pointwise source located at $\mathbf{s} \in \Omega^+$, i.e. the wave u^{inc} is the Green's function centered at $\mathbf{s}$. The Fourier coefficients of the trace and normal derivative trace of u^{inc} on Γ are then given by the following proposition [47].

Proposition 5. *Let $\mathbf{s} \in \Omega^+$. We assume that the incident wave u^{inc} is the Green's function centered at $\mathbf{s}$*

$$\forall \mathbf{x} \in \mathbb{R}^2 \setminus \{\mathbf{s}\}, \qquad u^{inc}(\mathbf{x}) = G(\mathbf{x}, \mathbf{s}) = \frac{i}{4} H^{(1)}_0(k\|\mathbf{x} - \mathbf{s}\|).$$

The Fourier coefficients in $\mathscr{B}$ of the trace and normal derivative trace of the incident wave on Γ are respectively given by

$$\widetilde{\mathbf{U}}_m^p = \left(u^{inc}|_\Gamma, \Phi_m^p\right)_{L^2(\Gamma)} = \frac{i\pi a_p}{2} J_m(ka_p) H_m^{(1)}(kr_p(\mathbf{s}))\overline{\widetilde{\Phi}_m^p(\mathbf{s})}$$

and

$$(\mathrm{d}\widetilde{\mathbf{U}})_m^p = \left(\partial_{\mathbf{n}} u^{inc}|_\Gamma, \Phi_m^p\right)_{L^2(\Gamma)} = k\frac{i\pi a_p}{2} J'_m(ka_p) H_m^{(1)}(kr_p(\mathbf{s}))\overline{\widetilde{\Phi}_m^p(\mathbf{s})}.$$

4.4 Near- and far-fields evaluations

By using Graf's addition theorem [37, 47], we can compute the expression of the single- and double-layer potentials at a point $\mathbf{x}$ located in the propagation domain Ω^+.

Proposition 6. *Let $\rho \in L^2(\Gamma)$ and $\mu \in H^{1/2}(\Gamma)$ be two densities admitting the following decompositions in the Fourier basis $\mathscr{B}$*

$$\rho = \sum_{p=1}^{M}\sum_{m\in\mathbb{Z}} \rho_m^p \Phi_m^p \qquad \textit{and} \qquad \lambda = \sum_{p=1}^{M}\sum_{m\in\mathbb{Z}} \lambda_m^p \Phi_m^p.$$

Then, for any point $\mathbf{x}$ in the domain of propagation Ω^+, the single-layer potential reads

$$\mathscr{L}\rho(\mathbf{x}) = \sum_{p=1}^{M}\sum_{m\in\mathbb{Z}} \rho_m^p \mathscr{L}\Phi_m^p(\mathbf{x}) = \sum_{p=1}^{M}\sum_{m\in\mathbb{Z}} \rho_m^p \frac{i\pi a_p}{2} J_m(ka_p) H_m^{(1)}(kr_p(\mathbf{x}))\widetilde{\Phi}_m^p(\mathbf{x}),$$

and the double-layer potential can be expressed as

$$\mathscr{M}\lambda(\mathbf{x}) = \sum_{p=1}^{M}\sum_{m\in\mathbb{Z}} \lambda_m^p \mathscr{M}\Phi_m^p(\mathbf{x}) = -\sum_{p=1}^{M}\sum_{m\in\mathbb{Z}} \lambda_m^p \frac{i\pi k a_p}{2} J'_m(ka_p) H_m^{(1)}(kr_p(\mathbf{x}))\widetilde{\Phi}_m^p(\mathbf{x}).$$

Proposition 6 implies that, for any $\mathbf{x}$ in Ω^+,

$$u(\mathbf{x}) = \mathscr{L}\rho(\mathbf{x}) + \mathscr{M}\lambda(\mathbf{x}) = \sum_{p=1}^{M}\sum_{m\in\mathbb{Z}} \frac{i\pi a_p}{2}\left[\rho_m^p J_m(ka_p) + \lambda_m^p J'_m(ka_p)\right] H_m^{(1)}(kr_p(\mathbf{x}))\widetilde{\Phi}_m^p(\mathbf{x}).$$

For computing the far-field pattern, let us recall that the scattered field u admits the following general Helmholtz's integral representation: $u = \mathscr{L}\rho + \mathscr{M}\lambda$, where ρ and λ are two unknown densities. The meaning of these densities is fully related to the integral equation that is chosen for a given boundary-value problem. For example, for the EFIE, MFIE and CFIE for the Dirichlet problem, ρ is computed according to the chosen integral equation and $\lambda = 0$. In the polar coordinates system (r, θ) and by using an asymptotic expansion of u when $r \to +\infty$, the following relation holds [18]

$$\forall \theta \in [0, 2\pi], \qquad u(r,\theta) = \frac{e^{ikr}}{r^{1/2}}\left[a_{\mathscr{L}}(\theta) + a_{\mathscr{M}}(\theta)\right] + O\left(\frac{1}{r^{3/2}}\right),$$

where $a_{\mathscr{L}}$ and $a_{\mathscr{M}}$ are the radiated far-fields for the single- and double-layer potentials, respectively, defined for any angle θ of $[0, 2\pi]$ by

$$\begin{cases} a_{\mathscr{L}}(\theta) = \dfrac{1}{\sqrt{8k\pi}} e^{i\pi/4} \displaystyle\int_\Gamma e^{-ik\boldsymbol{\theta}\cdot\mathbf{y}} \rho(\mathbf{y}) \mathrm{d}\Gamma(\mathbf{y}), \\ a_{\mathscr{M}}(\theta) = \dfrac{1}{\sqrt{8k\pi}} e^{i\pi/4} \displaystyle\int_\Gamma -\frac{ik}{\|\mathbf{y}\|} \boldsymbol{\theta}\cdot\mathbf{y} e^{-ik\boldsymbol{\theta}\cdot\mathbf{y}} \lambda(\mathbf{y}) \mathrm{d}\Gamma(\mathbf{y}), \end{cases}$$

with $\boldsymbol{\theta} := (\cos(\theta), \sin(\theta))$. In addition, the Radar Cross Section (RCS) is defined by

$$\forall \theta \in [0, 2\pi], \quad \mathrm{RCS}(\theta) = 10 \log_{10} \left(2\pi \left| a_{\mathscr{L}}(\theta) + a_{\mathscr{M}}(\theta) \right|^2 \right) (\mathrm{dB}).$$

To optimize the far-fields computation, these relations can be written thanks to the inner product between two infinite vectors. Indeed, let us introduce $\widetilde{\mathbf{a}}_{\mathscr{L}} = ((\widetilde{\mathbf{a}}_{\mathscr{L}})^p)_{1\leqslant p\leqslant M}$ and $\widetilde{\mathbf{a}}_{\mathscr{M}} = ((\widetilde{\mathbf{a}}_{\mathscr{M}})^p)_{1\leqslant p\leqslant M}$, where $(\widetilde{\mathbf{a}}_{\mathscr{L}})^p$ and $(\widetilde{\mathbf{a}}_{\mathscr{M}})^p$ are given by: $\forall p = 1, \ldots, M$,

$$\begin{cases} (\widetilde{\mathbf{a}}_{\mathscr{L}})^p = \left((\widetilde{\mathbf{a}}_{\mathscr{L}})^p_m \right)_{m\in\mathbb{Z}}, \qquad (\widetilde{\mathbf{a}}_{\mathscr{L}})^p_m = \dfrac{ie^{-i\pi/4}\sqrt{a_p}}{2\sqrt{k}} e^{-ib_p k\cos(\theta-\alpha_p)} J_m(ka_p) e^{im(\theta-\pi/2)}, \\ (\widetilde{\mathbf{a}}_{\mathscr{M}})^p = \left((\widetilde{\mathbf{a}}_{\mathscr{M}})^p_m \right)_{m\in\mathbb{Z}}, \qquad (\widetilde{\mathbf{a}}_{\mathscr{M}})^p_m = \dfrac{ie^{-i\pi/4}\sqrt{ka_p}}{2} e^{-ib_p k\cos(\theta-\alpha_p)} J'_m(ka_p) e^{im(\theta-\pi/2)}. \end{cases}$$

Then, we obtain the following: $a_{\mathscr{L}}(\theta) = (\widetilde{\mathbf{a}}_{\mathscr{L}})^T \widetilde{\boldsymbol{\rho}}$ and $a_{\mathscr{M}}(\theta) = (\widetilde{\mathbf{a}}_{\mathscr{M}})^T \widetilde{\boldsymbol{\lambda}}$.

5 Finite-dimensional approximations and numerical solutions proposed in μ-diff

We now have all the ingredients to numerically solve the four integral equations EFIE, MFIE, CFIE and BWIE, for sound-soft obstacles. In fact, any integral equation for any boundary condition can be solved according to the previous developments. In practice, the infinite Fourier systems need to be truncated to get a finite dimensional problem: we must pass from a sum over $m \in \mathbb{Z}$ to a finite number of Fourier modes that depends on ka_p, $p = 1, ..., M$. Let us consider e.g. the EFIE, the extension to the other boundary integral operators being direct. The EFIE is given by equation (8): $\widetilde{\mathbb{L}}\widetilde{\boldsymbol{\rho}} = -\widetilde{\mathbf{U}}$. To truncate each Fourier series associated with $(\Phi^p_m)_{m\in\mathbb{Z}}$ for the obstacle Ω_p^-, we only keep $2N_p+1$ modes in such a way that the indices m of the truncated series satisfy: $\forall p = 1, \ldots, M$, $-N_p \leqslant m \leqslant N_p$. The truncation parameter N_p must be fixed large enough, with $N_p \geqslant ka_p$, for $p = 1, ..., M$. An example [3, 8] is: $N_p = ka_p + C_p$, where C_p weakly grows with ka_p. A numerical study of the parameter N_p is proposed in [3, 8] where the following formula leads to a stable and accurate computation for *non penetrable scatterers*

$$N_p = \left[ka_p + \left(\frac{1}{2\sqrt{2}} \ln(2\sqrt{2}\pi ka_p \varepsilon^{-1}) \right)^{\frac{2}{3}} (ka_p)^{1/3} + 1 \right], \tag{9}$$

where ε is a small parameter (related to the relative tolerance required in the iterative Krylov subspace solver used for solving the truncated linear system (10), see [3, 8]) and $[r]$ denotes the integer part of a real-valued number r. In the case of penetrable obstacles, then the formulae should be adapted so that enough modes are considered for an accurate computation. Let us also remark

that very close scatterers are possible (see the numerical simulations given in [3]) but they cannot be sticky.

The resulting linear system writes

$$\mathbb{L}\boldsymbol{\rho} = -\mathbf{U}, \tag{10}$$

where we introduced the block matrix $\mathbb{L} = (\mathbb{L}^{p,q})_{1\leqslant p,q\leqslant M}$ and the vectors $\boldsymbol{\rho} = (\boldsymbol{\rho}^p)_{1\leqslant p\leqslant M}$ and $\mathbf{U} = (\mathbf{U}^p)_{1\leqslant p\leqslant M}$ defined by

$$\mathbb{L} = \begin{bmatrix} \mathbb{L}^{1,1} & \mathbb{L}^{1,2} & \dots & \mathbb{L}^{1,M} \\ \mathbb{L}^{2,1} & \mathbb{L}^{2,2} & \dots & \mathbb{L}^{2,M} \\ \vdots & \vdots & \ddots & \vdots \\ \mathbb{L}^{M,1} & \mathbb{L}^{M,2} & \dots & \mathbb{L}^{M,M} \end{bmatrix}, \qquad \boldsymbol{\rho} = \begin{bmatrix} \boldsymbol{\rho}^1 \\ \boldsymbol{\rho}^2 \\ \vdots \\ \boldsymbol{\rho}^M \end{bmatrix}, \qquad \mathbf{U} = \begin{bmatrix} \mathbf{U}^1 \\ \mathbf{U}^2 \\ \vdots \\ \mathbf{U}^M \end{bmatrix}. \tag{11}$$

For $p, q = 1, \dots, M$, the complex-valued matrix $\mathbb{L}^{p,q}$ is of size $(2N_p+1)\times(2N_q+1)$ and its coefficients $\mathbb{L}^{p,q}_{m,n}$ are: $\mathbb{L}^{p,q}_{m,n} = \widetilde{\mathbb{L}}^{p,q}_{m,n}$, for $m = -N_p, \dots, N_p$, $n = -N_q, \dots, N_q$. The complex-valued components of the vector $\boldsymbol{\rho}^p = (\boldsymbol{\rho}^p_m)_{-N_p\leqslant m\leqslant N_p}$ of size $2N_p + 1$ are the approximate Fourier coefficients ρ^p_m of ρ. For the sake of conciseness, we keep on writing: $\boldsymbol{\rho}^p_m = \widetilde{\boldsymbol{\rho}}^p_m = \rho^p_m$, for all $m = -N_p, \dots, N_p$. The complex-valued vector $\mathbf{U}^p = (\mathbf{U}^p_m)_{-N_p\leqslant m\leqslant N_p}$ is composed of the $2N_p + 1$ Fourier coefficients of the trace of the incident wave on Γ, i.e. $\mathbf{U}^p_m = \widetilde{\mathbf{U}}^p_m = \left(u^{\rm inc}|_\Gamma, \Phi^p_m\right)_{L^2(\Gamma)}$, $\forall m = -N_p, \dots, N_p$. If $N_{\rm tot} = \sum_{p=1}^M (2N_p+1)$ denotes the total number of modes, the size of the complex-valued matrix $\mathbb{L}$ is then $N_{\rm tot}\times N_{\rm tot}$. More generally, all the boundary integral operators can be truncated according to this process. Concerning the notations, it is sufficient to formally omit the tilde symbol $\sim$ over the quantities involved in sections (4.2)-(4.4).

Since the four finite-dimensional matrices $\mathbb{L}$, $\mathbb{M}$, $\mathbb{N}$ and $\mathbb{D}$ that respectively correspond to the four boundary integral operators L, M, N and D can be computed, the linear systems that approximate the EFIE, MFIE, CFIE and BWIE can be stated. For example, the CFIE leads to (with $0 \leqslant \alpha \leqslant 1$ and $\Im(\eta) \neq 0$)

$$\left[\alpha\eta\mathbb{L} + (1-\alpha)\left(\frac{\mathbb{I}}{2} + \mathbb{N}\right)\right]\boldsymbol{\rho} = -\alpha\eta\mathbf{U} - (1-\alpha)\mathrm{d}\mathbf{U}. \tag{12}$$

Let us remark that the matrix obtained after discretization is always a linear combination of the four integral operators $\mathbb{L}$, $\mathbb{M}$, $\mathbb{N}$, $\mathbb{D}$ and the identity matrix $\mathbb{I}$. As a consequence, for a given integral equation, the resulting matrix is of size $N_{\rm tot}\times N_{\rm tot}$ and has the same block structure as e.g. $\mathbb{L}$ (see equation (11)). The finite-dimensional linear system (10) (or (12)) is accurately solved in μ-diff by using the Matlab direct solver or a preconditioned Krylov subspace linear solver that uses fast matrix-vector products based on Fast Fourier Transforms (FFTs), the choice of the linear algebra strategy (direct vs. iterative) depending on the configuration with respect to ka_p and M. The preconditioner included in μ-diff is based on the diagonal of the integral operator matrix representation which is solved and corresponding to single scattering. The use of FFTs is made possible since the off-diagonal blocks of the integral operators can be written as the products of diagonal and Toeplitz matrices [3, 8] (see e.g. the matrices $\widetilde{\mathbb{S}}^{p,q}_{m,n}$ in section 4.2). In addition, low memory is only necessary when ka_p is large enough since the storage of the Toeplitz matrices can be optimized. This resulting storage technique is called *sparse* representation in μ-diff, in contrast with the *dense* (full) storage of the complex-valued matrices. Let us assume that $a_p \approx a$, for $1 \leqslant p \leqslant M$. In terms of storage, the full matrix version requires to store about $4M^2[ka]^2$ coefficients (assuming that N_p are fixed by formula (9), and $[r]$ denotes the integer part of a real number r) while the

sparse storage needs about $4M^2[ka]$ complex-valued coefficients. In terms of computational time for solving the linear system, the direct (multithreaded) gaussian solver included in Matlab leads to a cost that scales with $\mathcal{O}(M^3(ka)^3)$. For the preconditioned iterative Krylov subspace methods (e.g. restarted GMRES), the global cost is $\mathcal{O}(M^2 ka \log_2(ka))$, the converge rate depending on the physical situation and robustness of the preconditioner. From these remarks, we deduce that an iterative method is an efficient and cheap alternative to a direct solver for large wavenumbers ka, but also for large M. We refer to [3, 8] for a thorough computational study of the various numerical strategies. A few examples in μ-diff are provided (see section 7 and the corresponding scripts) with the toolbox. Finally, the post-processing formulas (near- and far-fields quantities) clearly inherits of the truncation procedure (see section 4.4).

6 Structure of the μ-diff Matlab toolbox

Because μ-diff includes all the integral operators that are needed in scattering (traces and normal derivative traces of the single- and double-layer potentials), a large class of scattering problems can be solved. Concerning the geometrical configurations, any deterministic or random distribution of disks is possible. Finally, μ-diff includes post-processing facilities like *e.g.*: surface and far-fields computations, total and scattered exterior (near-field) visualization...

We now introduce the μ-diff Matlab toolbox by explaining the main predefined functions and their relations with the previous mathematical derivations. Section 6.1 shows how to define the scattering configuration (geometry and physical parameters). Section 6.2 presents the way the integral equations must be defined and solved. Finally, section 6.3 describes the data post-processing. To be concrete, we propose to fully treat in section 7.1 the example of multiple scattering by a collection of randomly distributed sound-soft and sound-hard circular cylinders based on the EFIE. Section 7.2 presents an example of scattering by penetrable obstacles and a more advanced example is considered in section 7.3 for time reversal in homogeneous media.

The μ-diff toolbox is organized following the five subdirectories:

- `mudiff/PreProcessing/`: pre-processing data functions (incident wave and geometry) (section 6.1).
- `mudiff/IntOperators/`: functions for the four basic integral operators (full matrix and sparse structure) used in the definition of the integral equations to solve (section 6.2).
- `mudiff/PostProcessing/`: post-processing functions of the solution (trace and normal derivative traces, computation of the scattered/total wavefield at some points of the spatial domain or on a grid, far-field and RCS) (section 6.3).
- `mudiff/Common/`: this directory includes functions that are used in μ-diff but which does not need to be known from the standard user point of view.
- `mudiff/Examples/`: various scripts are presented for the user in standard configurations.

In addition, the μ-diff user-guide can be found under the directory `mudiff/Doc/`.

6.1 Pre-processing: physical and geometrical configurations

All the pre-processing functions are included in the directory `mudiff/PreProcessing/`.

The pre-processing (`mudiff/PreProcessing/IncidentWave`) in μ-diff consists first in defining the scattering parameters (incidence angle β or location of the point source, wavenumber k). This provides the possibility of defining the traces and normal derivative traces of the incident wavefield through the global function `IncidentWave` (plane wave or point sources), or through the specific functions `PlaneWave`, `DnPlaneWave` (plane wave), `PointSource`, `DnPointSource` (point source) in view of writing any integral formulation. The global function also allows to build a vector mixing the trace and normal derivative trace of an incident wave (e.g. a vector combining `PlaneWave` and `DnPlaneWave`). Let us also note that the user could define its own incident field in the Fourier basis $\mathscr{B}$ by sampling the signal and truncating.

Next, the geometrical configuration can be described thanks to functions available in the directory
`mudiff/PreProcessing/Geometry`. The user can define himself the centers and radii (`(O, a)`) of the circular cylinders, create a rectangular (`RectangularLattice` function) or triangular (`TriangularLattice` function) lattice of circular cylinders or can even build a random set of cylinders in a rectangular domain (`CreateRandomDisks` function), specifying many geometrical parameters to describe dilute or dense random media (minimal and maximal size of the disks, minimal distance between each disk,...) and even create holes in the domain where no disk must overlap (this can be interesting for example for numerically building photonics crystals with cavity).

6.2 Defining and solving an integral equation

The functions defining the integral operators are in the directory `mudiff/IntOperators/` which has the `Dense/` and `Sparse/` subdirectories for the matrix and sparse (@function) representations of the four basic integral operators used in scattering, i.e. $\mathbb{L}$, $\mathbb{M}$, $\mathbb{N}$ and $\mathbb{D}$. Preconditioned versions of the operators by their diagonal part are also defined (based on single scattering [3, 8, 48]). For example, for a Dirichlet boundary value problem, the EFIE (6), which is based on a single-layer representation, can be built by using the function `SingleLayer` for a full matrix version or the function `SpSingleLayer` to get a sparse representation. Nevertheless, from the user point of view, there is no need to enter into the detail of all the related functions. Indeed, a common interface, called `IntegralOperator`, allows to directly build a linear combination of the previous integral operators, which are all indexed by a hard-coded number. This provides a very convenient way when one does not want to use the specific functions or need to build a more complicated operator. For example, the spectral (matrix) construction of the BWIE for the Dirichlet problem can be written

```
IntegralOperator(O, a, M_modes, k, [1, 2, 3], [0.5, -eta, -1]);
```
(13)

for

$$\frac{1}{2}\mathbb{I} - \eta\mathbb{L} - \mathbb{M}, \tag{14}$$

where `O` and `a` are respectively the centers and radii of the M circular cylinders. The vector `M_modes` is such that `M_modes(p)`$= N_p$, the argument vector `[1, 2, 3]` refers to respectively the operators Identity (`1`), L (`2`) and M (`3`) and the last one `[0.5, -eta, -1]` carries the weight to apply to each operator in the linear combination (`eta` must previously have taken a prescribed complex value in

the script). Without entering too much into details, each block of the final global matrix can be specified thanks to this numbering (instead of a vector, a 2D- or a 3D-array is then considered as argument). In the same way, the other operators can be called either by `IntegralOperator` and their numbering: null matrix (0), N (4), D (5) and the preconditioned version for a Dirichlet (6) and Neumann (7) problem, or directly by their interfaced functions (`DnSingleLayer`, `DnDoubleLayer`, `PrecondDirichlet` and `PrecondNeumann`).

Once the matrix representation of the integral operator has been defined and the right-hand side has been computed, then the integral equation can be solved. For the matrix representation of the integral operator, it is possible to use a direct Gauss solver (based on the backslash \ Matlab operator) or any iterative Krylov subspace solver available in Matlab (GMRES, BiCGStab, ...).

```
Uinc = PlaneWave(O, a, M_modes, k, beta_inc);
BWIE = IntegralOperator(O, a, M_modes, k, [1, 2, 3], [0.5, -eta, -1]);
psi = BWIE\Uinc;% direct solving
```

For the sparse version, the operators are stored using the Matlab `cell` structure and there is moreover no other possibility than using an iterative solver (the matrix is not fully stored). Building a linear combination of the different integral operators becomes then slightly different: the `SpIntegralOperator` function cannot linearly combine the integral operators as in equation (13), due to a possible loss of the structure. The solution we propose is to assemble each operator separately and combine them at each (sparse) matrix-vector product, using the dedicated function `SpMatVec`. For the BWIE, the following syntax is required to build the function representing the integral operator (14) which is next called for solving the equation (7) by using the restarted GMRES Matlab solver and the sparse matrix-vector product `SpMatVec`:

```
Uinc = PlaneWave(O, a, M_modes, k, beta_inc);
SpI = SpIdentity(O, a, M_modes);
SpL = SpSingleLayer(O, a, M_modes, k);
SpM = SpDoubleLayer(O, a, M_modes, k);
[psi_SpBW,FLAG_SpBW,RELRES_SpBW,ITER_SpBW,RESVEC_SpBW] =...
          gmres(@(X)SpMatVec(X,M_modes, {SpI, SpL, SpM}, [0.5, -eta_BW, -1]),...
                        Uinc, RESTART, TOL, MAXIT, [], []);
```

Let us note that, first, the functions `SpIdentity`, `SpSingleLayer` and `SpDoubleLayer` in fact, call `SpIntegralOperator` with the right label (resp. 1, 2 and 3), and second the way μ-diff is built allows to define the matrices and vectors block-by-block and thus to solve any integral equation formulation which can for example take into account different boundary conditions on the circular cylinders, complex wavenumber for the interior/exterior of a disk,...

6.3 Post-processing of computed outputs

Once the (physical or fictitious) surface density has been computed as the solution to the integral equation, all the post-processing facilities described in section 4.4 are available. Note that computing the trace or normal derivative trace of the wavefield on the boundary of one of the disk depends on the integral representation of the scattered field, and generally only implies a linear combination of the four boundary integral operators.

The post-processing functions are defined in the subdirectory `mudiff/PostProcessing/`. The function `PlotCircles` allows to display the geometrical configuration given by the collection of

disks. Functions related to the near-field are given by `ExternalPotential` and `InternalPotential` if one wants to compute the solution at a point of the domain or on a whole grid, from the exterior or interior of the scatterers, respectively. In addition, far-fields can be obtained by applying the `FarField` function. For the Radar Cross Section, the μ-diff function is called `RCS`. Each of these functions needs the integral representation of the scattered field. To help the user, each function has an interface function for the single- and the double-layer potential only (e.g. `ExternalSingleLayerPotential`, `FarFieldSingleLayer`, ...). Even if the far-field is efficiently computed, the user should be aware that the computation of the volume potentials on a huge discrete grid can need more time than assembling and solving the linear system.

The reader can find in the example subdirectory `mudiff/Examples/Benchmark` many examples of manipulation of the code in the files `BenchmarkDirichlet` (sound-soft scattering) and `BenchmarkNeumann` (sound-hard scattering). An effort has been made to show all the possible combinations of operators available in μ-diff, trying to use the main functions. The user can clearly play with the parameters sets, the only limit being given by the memory of the computer used. The notation concerning the integral equations are related to the present paper (EFIE, MFIE, CFIE, BWIE).

7 Numerical examples with μ-diff

7.1 Example I: scattering by randomly distributed sound-soft or sound-hard circular cylinders

To show an example of problem solved by μ-diff, we consider that we use the EFIE to solve the scattering problem by a collection of sound-soft or sound-hard randomly distributed scatterers. The corresponding script (`BenchmarkDN`) for simulating the results of this section is available in the examples directory.

We consider a plane wave (for a wavenumber $k = 6\pi$ and an incidence angle $\beta = 0$ (rad.)) that scatterers on a collection of $M = 360$ circular cylinders (see figure 2(a)). These disks are randomly distributed in a square domain $[-3; 3]^2$. In addition, their radii are such that $a_{\min} := 10^{-1} \leqslant a_p \leqslant a_{\max} := 1.5 \times 10^{-1}$, the minimal distance between the disks is $d_{\min} := 0.01 \times a_{\min}$. The number of modes is fixed by the formula (9), taken from (21) in [3]. The trace and normal derivative trace of the incident plane wave are then defined to build the right-hand sides of the EFIE. We report in figure 2(b) the RCS for the sound-soft and sound-hard acoustic problems. These pictures show that the far-fields have some very different structures. In addition, the amplitudes of total and scattered wavefields are displayed on figures 2(c)-2(d) for the sound-soft problem and figures 2(e)-2(f) for the sound-hard problem. We consider a larger domain to show the wavefield behavior both inside and outside the cluster of circular cylinders. We observe in particular that there is almost no penetration of the incident field in the sound-soft case while scattering arises deeply in the sound-hard cluster.

7.2 Example II: multiple scattering by a cluster of homogeneous penetrable obstacles

Extending the previous example, the script `BenchmarkPenetrable` solves the transmission problem with penetrable obstacles. The wavenumber k is now piecewise constant with value k^+ outside the

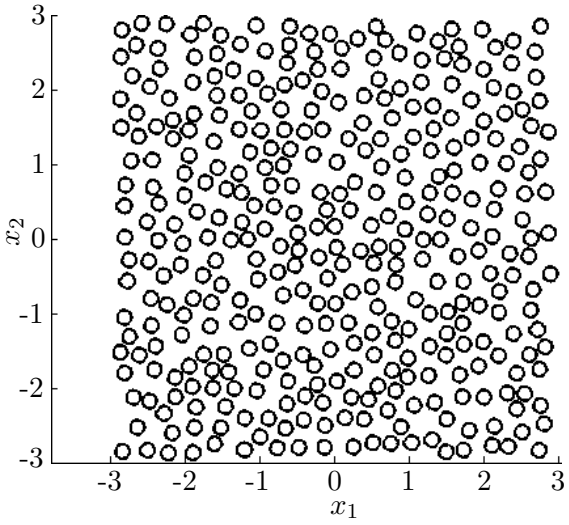

(a) Cluster of $M = 360$ disks

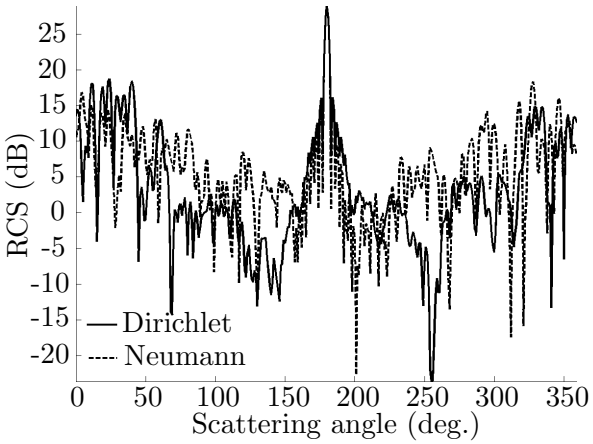

(b) RCS for the sound-soft and sound-hard cases

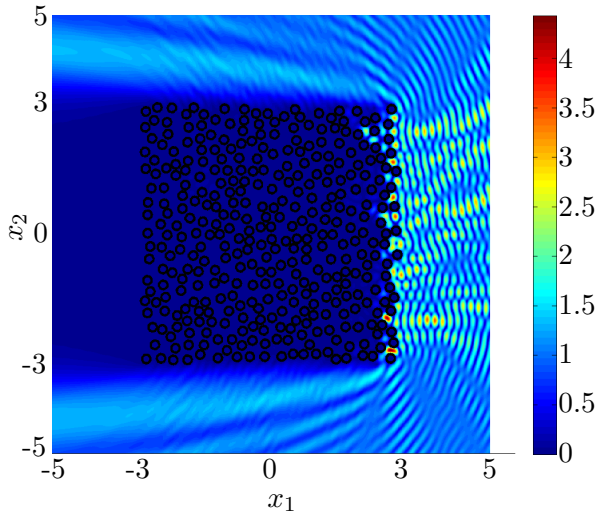

(c) Sound-soft problem: $|u^{\text{tot}}|$

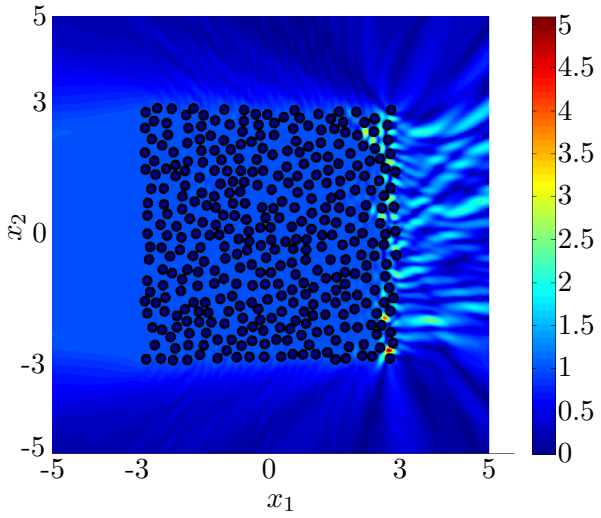

(d) Sound-soft problem: $|u|$

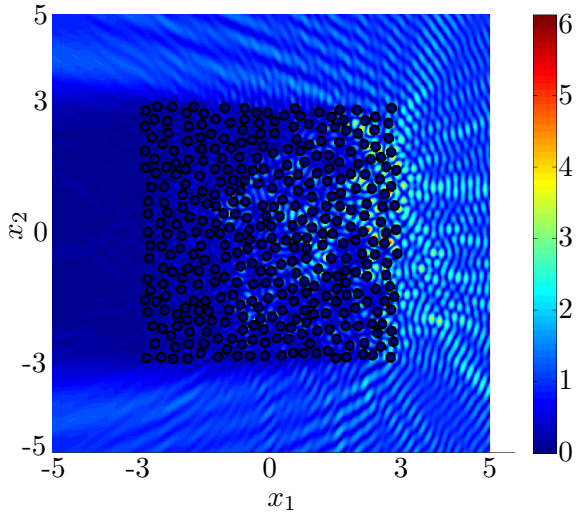

(e) Sound-hard problem: $|u^{\text{tot}}|$

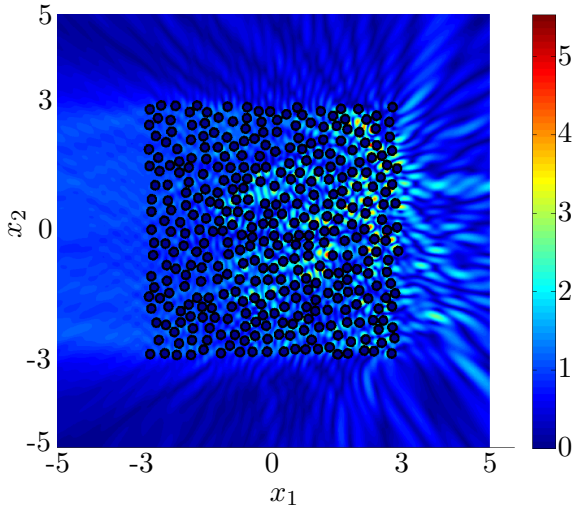

(f) Sound-hard problem: $|u|$

Figure 2: Multiple scattering of an incident plane wave ($k = 6\pi$ and $\beta = 0$ (rad.) (coming from the right)) by $M = 360$ sound-soft/sound-hard obstacles, randomly distributed in $[-3; 3]^2$.

obstacles and k^- inside. The scattered field u^+ and the transmitted wavefield u^- are then the solution to the following transmission boundary-value problem

$$\left\{\begin{array}{rcll} \Delta u^- + (k^-)^2 u^- & = & 0, & \text{in } \Omega^-, \\ \Delta u^+ + (k^+)^2 u^+ & = & 0, & \text{in } \Omega^+, \\ u^+ - u^- & = & -u^{\text{inc}}, & \text{on } \Gamma, \\ \partial_{\mathbf{n}} u^+ - \partial_{\mathbf{n}} u^- & = & -\partial_{\mathbf{n}} u^{\text{inc}}, & \text{on } \Gamma, \\ \lim\limits_{||\mathbf{x}||\to+\infty} ||\mathbf{x}||^{1/2} \left(\nabla u^+ \cdot \dfrac{\mathbf{x}}{||\mathbf{x}||} - ik^+ u^+ \right) = 0. & & & \end{array}\right. \tag{15}$$

The total (physical) field u^{tot} is given by $u^{\text{tot}} = u^+ + u^{\text{inc}}$ outside and by $u^{\text{tot}} = u^-$ inside the obstacles. To solve this problem through an integral equation, we consider a single-layer representation of the wavefields u^+ and u^-

$$u^+ = \mathscr{L}^+ \rho^+ \quad \text{and} \quad u^- = \mathscr{L}^- \rho^-, \tag{16}$$

where $\mathscr{L}^+$ (resp. $\mathscr{L}^-$) is the single-layer operator with wavenumber k^+ (respectively k^-). The pair of unknowns (ρ^+, ρ^-) is then the solution to the following integral equation

$$\begin{pmatrix} L^+ & -L^- \\ -\dfrac{I}{2} + N^+ & \left(\dfrac{I}{2} + N^-\right) \end{pmatrix} \begin{pmatrix} \rho^+ \\ \rho^- \end{pmatrix} = \begin{pmatrix} -u^{\text{inc}} \\ -\partial_{\mathbf{n}} u^{\text{inc}} \end{pmatrix}. \tag{17}$$

The plus or minus superscripts in L and N refers to as the exterior wavenumbers k^+ or k^-. Like for the sound-soft and sound-hard scattering problems, the far-field and the quantities u^+ and u^- can be computed, thanks to their respective single-layer representation (16). Let us remark that the present problem also arises for electromagnetic wave scattering by a collection of cylindrical obstacles, invariant and infinite in the z-direction. The wavenumbers are then given by $k^+ = \omega\sqrt{\varepsilon_0 \mu_0}$ and $k_p^- = \omega\sqrt{\varepsilon_p \mu_p}$, where ω is the pulsation of the wave and (ε_0, μ_0) (respectively (ε_p, μ_p)) are respectively the electric permittivity and electromagnetic permeability in the vacuum (respectively in the obstacle Ω_p^-). The boundary-value problem (15) remains the same except for the normal derivative of the wavefield which might be discontinuous at Γ_p. Indeed, for the transverse-magnetic mode (or transverse-electric mode), the unknown u represents the z-component of the magnetic field H and the transmission condition becomes: $\partial_{\mathbf{n}} u^+ - \frac{\varepsilon_0}{\varepsilon_p} \partial_{\mathbf{n}} u^- = -\partial_{\mathbf{n}} u^{\text{inc}}$, on Γ_p, whereas for the transverse-electric mode (or transverse-magnetic mode), then $u = E_z$ and the transmission condition reads as $\partial_{\mathbf{n}} u^+ - \frac{\mu_0}{\mu_p} \partial_{\mathbf{n}} u^- = -\partial_{\mathbf{n}} u^{\text{inc}}$. As a consequence, the integral equation (17) is modified by only multiplying the operator $(I/2 + N^-)$ by the parameter $\frac{\varepsilon_0}{\varepsilon}$ or $\frac{\mu_0}{\mu}$, depending on the polarization, where $\varepsilon|_{\Gamma_p} = \varepsilon_p$ and $\mu|_{\Gamma_p} = \mu_p$.

A numerical example solved by μ-diff is shown in figures 3(a)-3(d) for $M = 400$ unit penetrable unitary disks placed as a rectangular lattice centered on $(0, 0)$, which is also the location of a point source emitting a wave. The middle row and column, corresponding to centers with 0 abscissa and 0 ordinate respectively, have been removed. The whole geometry has been built thanks to the pre-processing μ-diff functions `RectangularLattice` and `RemoveDisk`. This last function deletes easily some disks in a geometrical configuration if they are not needed. The exterior wavenumber is set to $k^+ = 1$ and the wavenumber k^- inside the obstacles is equal to $k^- = 2k^+ = 2$. We report the RCS, as well as the amplitude, real and imaginary parts of the total field u^{tot}. Of course, more scatterers, higher frequencies and complex-valued wavenumbers could be chosen when launching a simulation with μ-diff.

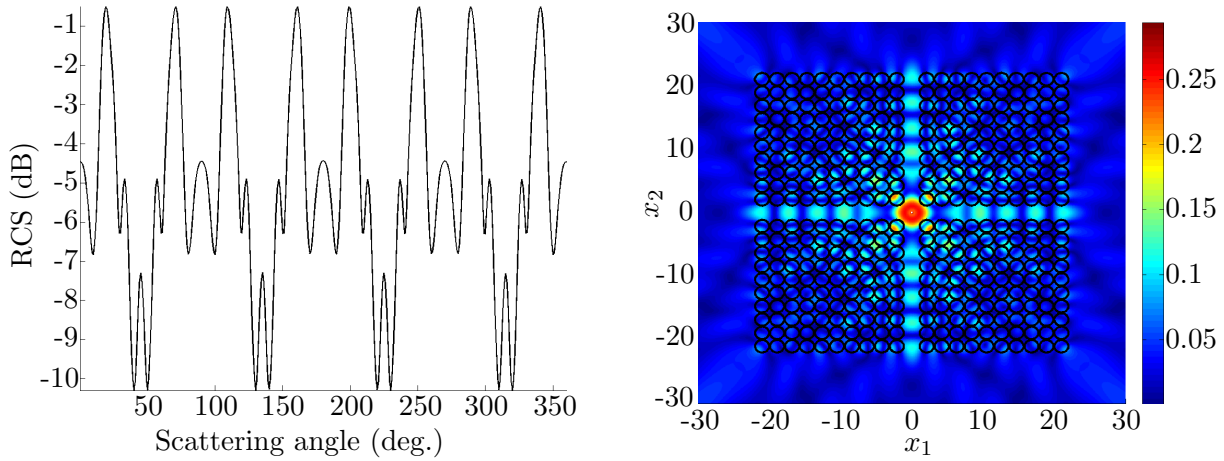

(a) RCS for the penetrable case

(b) Penetrable problem: $\left|u^{\text{tot}}\right|$

(c) Penetrable problem: $\Re(u^{\text{tot}})$

(d) Penetrable problem: $\Im(u^{\text{tot}})$

Figure 3: Scattering of a point source (located at the origin) by a collection of $M = 400$ penetrable unit disks (interior wavenumber $k^- = 2k$, with the exterior wavenumber $k = 1$).

7.3 Example III: a more advanced application in time reversal

Finally, a last numerical example related to the use of μ-diff concerns an inverse scattering problem. Time reversal is a technique based on the reversibility property of the wave equation in a non dissipative medium to send back a signal in the original medium and on the source that first emitted it. The goal is to get informations about the medium. Time reversal methods do not provide a full characterization of the medium but lead to some useful informations about the presence of failures or obstacles in the medium. Physical time reversal experiments are possible since the pioneering developments of the Time Reversal Mirror (TRM) by Fink and his team [26]. These devices are composed by numerous cells that can play alternatively the role of emitters or receivers. A typical time reversal experiment can be described as follows: a point source emits a wave in the medium, the mirror measures it, time-reverses it and sends it back to the medium. The resulting back-propagated wave is expected to focus on the source both in space and time, with a resolution depending on various parameters such as the size, the position or the distance of the mirror to the source, the medium,... (without being exhaustive, we refer for instance to [10, 25], the literature on this topic being huge).

Based on this idea, the DORT method (french acronym for "Decomposition of the Time Reversal Operator"), developed by Prada and Fink [27, 43], aims to detect and locate non-emitting objects. In fact, this technique go further than the pure detection since it also generates waves that focus selectively on the obstacles that are supposed to be small and distant enough from each other. The fascinating applications of the DORT are numerous. Let us mention among others the imaging and the destruction of kidney stones [38, 49] or subsurface imaging [11] by using the DORT as a filter. The method is based on the iteration of the following cycle: first the TRM emits a wave toward the obstacles, generating a scattered wave which is then measured by the TRM and time-reversed. This cycle - "emission, reception and time-reversal" - is then repeated again by sending back the time-reversed measurements. After many iterations, it appears that the back propagated wave focuses on the most reflecting obstacle. To detect and focus waves on the other obstacles, the DORT method consists in 1) building the so-called Time Reversal Operator (TRO), designated by $\mathcal{T}$ here and defined by two cycles "emission-reception-time reversal", and 2) study its spectral properties. Indeed, when the obstacles are small and sufficiently far to each other, this operator has as much significant eigenvalues as the number of obstacles, and moreover, the associated eigenfunctions can be used to generate waves that focus selectively on the obstacles. This has been proved mathematically in the far-field context for sound-hard acoustic scattering in [32] and studied numerically by using an earlier basic version of the μ-diff toolbox in [47]. These results have also been extended to other types of waves such as the dielectric cases in [13] for which numerical simulations have been performed.

For the sake of simplicity, we only present here the acoustic far-field case, even if the scripts for the two cases are available in the `Examples/TimeReversal/FarField` directory of the current μ-diff toolbox. For this case, the time reversal mirror is placed at infinity and totally surrounds the obstacles. In particular, this implies that the TRM sends a linear combination of plane waves, called Herglotz waves, and measures the scattered far-field. More precisely, an Herglotz wave u_I with parameter f is given by

$$u_I(x_1, x_2) = \int_0^{2\pi} f(\alpha) e^{ik(x_1 \cos(\alpha) + x_2 \sin(\alpha))} \, \mathrm{d}\alpha.$$

Let us denote by $\mathcal{F}f$ the far-field generated by an Herglotz wavefield of parameter f. Then, it

can be proved [32] that the TRO is given by: $\mathcal{T} = \mathcal{F}^*\mathcal{F}$, where $\mathcal{F}^*$ is the adjoint operator of $\mathcal{F}$. An eigenfunction g of $\mathcal{T}$ can then be used as a parameter of an Herglotz wavefunction to generate a wave focusing on the obstacles if its associated eigenvalue is significantly large. In the discrete context, building the matrix $\mathbb{T}$ associated with the operator $\mathcal{T}$ can be done as follows. First, the TRM is discretized by using N_α points or angles α_j, $j = 1, ..., N_\alpha$ (note that, if a point emits an incident wave with angle α, then the TRM measures the far-field in the opposite direction $\alpha + \pi$). A discrete Herglotz wave emitted by the mirror is then

$$u_I(x_1, x_2) = \sum_{j=1}^{N_\alpha} h_\alpha f_j e^{ik(x_1 \cos(\alpha_j) + x_2 \sin(\alpha_j))},$$

where $f_j = f(\alpha_j)$ and h_α is the discretization step. The algorithm to obtain the time-reversal matrix $\mathbb{T}$ is then : for every angle α_j, the scattered field is computed and its associated far-field is calculated at every reception angle $(\alpha_i + \pi)$, $i = 1, \ldots, N_\alpha$. This leads to a vector of size N_α which is stored as the j^{th} column of a matrix $\mathbb{F}$ of size $N_\alpha \times N_\alpha$. For i, j, the quantity $\mathbb{F}(i, j)$ hence corresponds to the far-field in the direction $\alpha_i + \pi$ of the scattered field generated by an incident plane wave of direction α_j. Once the N_α emission angles have been considered, the matrix $\mathbb{F}$ is a discrete representation of the far-field operator and the matrix $\mathbb{T}$ is obtained by the relation: $\mathbb{T} = \overline{\mathbb{F}}^T \mathbb{F}$.

All the elementary operations described above can be easily coded by using μ-diff and the Matlab function `eigen` which provides the eigenvalues and eigenvectors of $\mathbb{T}$. The Herglotz waves are computed thanks to the function `HerglotzWave` available in the μ-diff directory related to the examples. Finally, running the script `DORT_NonPenetrable.m` generates a DORT experiment. An example is given on figures 4(a)-4(d). We consider a medium with three penetrable circular scatterers, with centers $[0, 20]$, $[10, -10]$, $[-10, -20]$ and respective radius 0.02, 0.01, 0.005. The wavenumber is equal to $k = 2\pi$. As shown on figure 4(a), the time reversal matrix $\mathbb{T}$ has three significant eigenvalues. We report on figures 4(b)-4(d) the amplitude of the Herglotz wavefunctions associated with the three largest eigenvalues. We clearly observe that they selectively focus on the obstacles, from the most to the less reflecting (or largest) one.

8 Conclusion

This paper presented a new flexible, efficient and robust Matlab toolbox called μ-diff[†]. This open source code is based on the theory of integral representations for solving two-dimensional multiple scattering problems by many circular cylinders. The spectral approximation method uses Fourier series expansion and efficient linear algebra algorithms in conjunction with optimized memory storage techniques for solving the finite-dimensional approximate integral formulations. Pre- and post-processing facilities are included in μ-diff (near- and far-fields representations, surface fields). All the features are described with enough details so that the user can directly solve complex problems related to physics or engineering applications. In addition, we provide some benchmark scripts that reproduce the simulations shown in this paper (direct and inverse scattering). The μ-diff toolbox is developed in such a way that a wide class of multiple scattering problems by disks can be solved.

[†] `http://mu-diff.math.cnrs.fr`

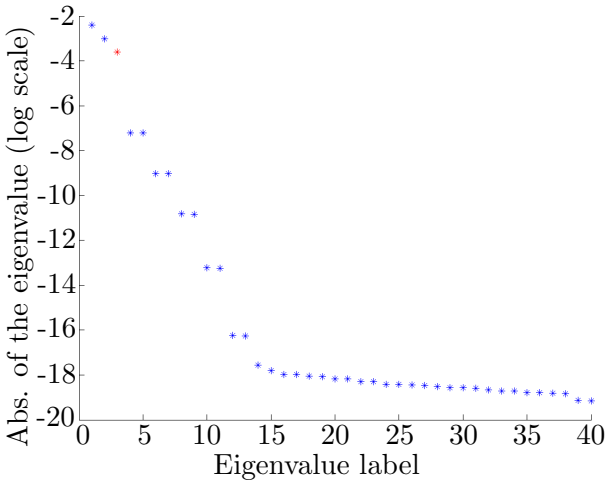

(a) 40 largest eigenvalues of T (log scale of their absolute value)

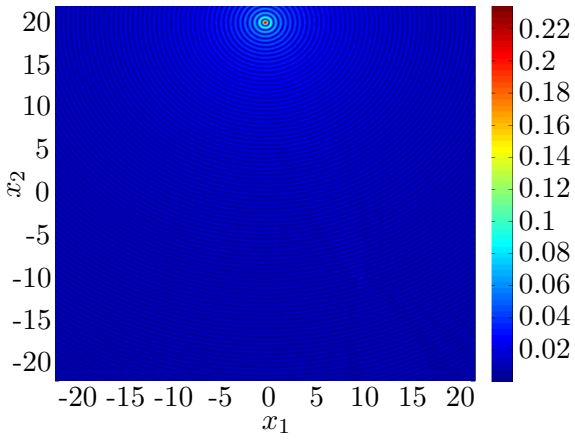

(b) Absolute value of the first Herglotz wavefunction

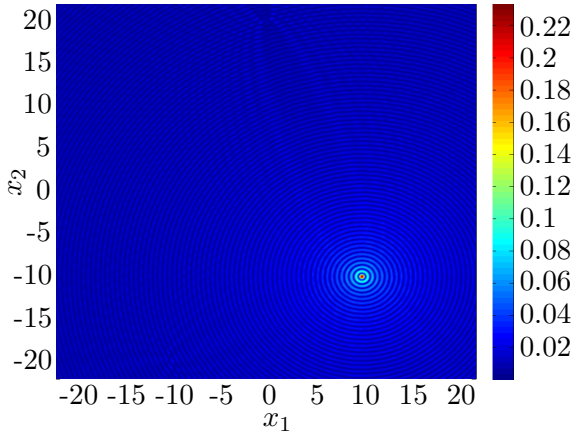

(c) Absolute value of the second Herglotz wavefunction

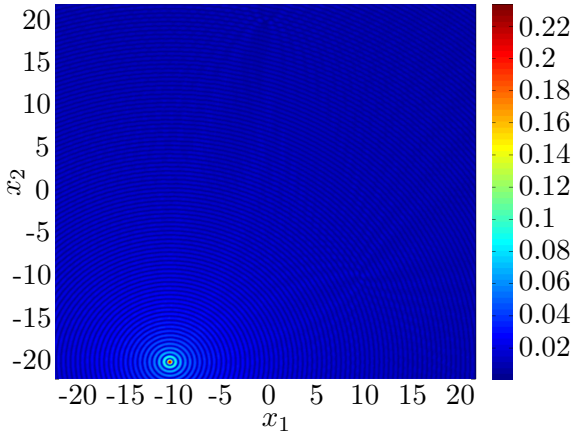

(d) Absolute value of the third Herglotz wavefunction

Figure 4: DORT: an example of numerical experiment obtained by using μ-diff.

Acknowledgements. This work has been funded by the Institute of Scientific Research and Revival of Islamic Heritage at Umm Al-Qura University (project ID 43405027).

References

[1] S. Acosta. On-surface radiation condition for multiple scattering of waves. *Computer Methods in Applied Mechanics and Engineering*, 283:1296–1309, 2015.

[2] S. Acosta and V. Villamizar. Coupling of Dirichlet-to-Neumann boundary condition and finite difference methods in curvilinear coordinates for multiple scattering. *J. Comput. Phys.*, 229(5498-5517), 2010.

[3] X. Antoine, C. Chniti, and K. Ramdani. On the numerical approximation of high-frequency acoustic multiple scattering problems by circular cylinders. *J. Comput. Phys.*, 227(3):1754–1771, 2008.

[4] X. Antoine and M. Darbas. Alternative integral equations for the iterative solution of acoustic scattering problems. *Quaterly J. Mech. Appl. Math.*, 1(58):107–128, 2005.

[5] X. Antoine and M. Darbas. Generalized combined field integral equations for the iterative solution of the three-dimensional Helmholtz equation. *M2AN Math. Model. Numer. Anal.*, 1(41):147–167, 2007.

[6] X. Antoine and M. Darbas. *Integral Equations and Iterative Schemes for Acoustic Scattering Problems*. to appear, 2015.

[7] X. Antoine, C. Geuzaine, and K. Ramdani. *Wave Propagation in Periodic Media - Analysis, Numerical Techniques and Practical Applications*, volume 1, chapter Computational Methods for Multiple Scattering at High Frequency with Applications to Periodic Structures Calculations, pages 73–107. Progress in Computational Physics, 2010.

[8] X. Antoine, K. Ramdani, and B. Thierry. Wide frequency band numerical approaches for multiple scattering problems by disks. *J. Algorithms Comput. Technol.*, 6(2):241–259, 2012.

[9] S. Bidault, F.J.G. de Abajo, and A. Polman. Plasmon-based nanolenses assembled on a well-defined DNA template. *Journal of the American Chemical Society*, 130(9):2750–2751, 2008.

[10] L. Borcea, G. Papanicolaou, and C. Tsogka. A resolution study for imaging and time reversal in random media. In *Inverse problems: theory and applications (Cortona/Pisa, 2002)*, volume 333 of *Contemp. Math.*, pages 63–77. Amer. Math. Soc., Providence, RI, 2003.

[11] L. Borcea, G. Papanicolaou, and C. Tsogka. Adaptive time-frequency detection and filtering for imaging in heavy clutter. *SIAM J. Imaging Sciences*, 4(3):827–849, 2011.

[12] H. Brakhage and P. Werner. Über das Dirichletsche Aussenraumproblem für die Helmholtzsche Schwingungsgleichung. *Arch. Math.*, 16:325–329, 1965.

[13] C. Burkard, A. Minut, and K. Ramdani. Far field model for time reversal and application to selective focusing on small dielectric inhomogeneities. *Inverse Problems and Imaging*, 7(2):445–470, 2013.

[14] A. J. Burton and G. F. Miller. The application of integral equation methods to the numerical solution of some exterior boundary-value problems. *Proc. Roy. Soc. London. Ser. A*, 323:201–210, 1971. A discussion on numerical analysis of partial differential equations (1970).

[15] M. Cassier and C. Hazard. Multiple scattering of acoustic waves by small sound-soft obstacles in two dimensions: Mathematical justification of the Foldy-Lax model. *Wave Motion*, 50(18-28), 2013.

[16] J.T. Chen, Y.T. Lee, Y.J. Lin, I.L. Chen, and J.W. Lee. Scattering of sound from point sources by multiple circular cylinders using addition theorem and superposition technique. *Numerical Methods for Partial Differential Equations*, 27(1365-1383), 2011.

[17] D. Colton and R. Kress. *Inverse Acoustic and Electromagnetic Scattering Theory*, volume 93 of *Applied Mathematical Sciences*. Springer-Verlag, Berlin, second edition, 1998.

[18] D. L. Colton and R. Kress. *Integral Equation Methods in Scattering Theory*. Pure and Applied Mathematics (New York). John Wiley & Sons Inc., New York, 1983. A Wiley-Interscience Publication.

[19] A. Devilez, B. Stout, N. Bonod, and E. Popov. Spectral analysis of three-dimensional photonic jets. *Optics Express*, 16(18):14200–14212, 2008.

[20] T.E. Doyle, D.A. Robinson, S.B. Jones, K.H. Warnick, and B.L. Carruth. Modeling the permittivity of two-phase media containing monodisperse spheres: Effects of microstructure and multiple scattering. *Physical Review B*, 76(5), 2007.

[21] T.E. Doyle, A.T. Tew, K.H. Warnick, and B.L. Carruth. Simulation of elastic wave scattering in cells and tissues at the microscopic level. *Journal of the Acoustical Society of America*, 125(3):1751–1767, 2009.

[22] M. Ehrhardt. *Wave Propagation in Periodic Media Analysis, Numerical Techniques and practical Applications, E-Book Series Progress in Computational Physics (PiCP), Volume 1*. Bentham Science Publishers, 2010.

[23] M. Ehrhardt, H. Han, and C. Zheng. Numerical simulation of waves in periodic structures. *Commun. Comput. Phys.*, 5:849–870, 2009.

[24] P. Ferrand, J. Wenger, A. Devilez, M. Pianta, B. Stout, N. Bonod, E. Popov, and H. Rigneault. Direct imaging of photonic nanojets. *Optics Express*, 16(10):6930–6940, 2008.

[25] M. Fink. Time-reversal acoustics. In *Inverse problems, multi-scale analysis and effective medium theory*, volume 408 of *Contemp. Math.*, pages 151–179. Amer. Math. Soc., Providence, RI, 2006.

[26] M. Fink. Time-reversal acoustics. *J. Phys.: Conf. Ser.*, 118(1):012001, 2008.

[27] M. Fink and C. Prada. Eigenmodes of the time-reversal operator: A solution to selective focusing in multiple-target media. *Wave Motion*, 20:151–163, 1994.

[28] C. Geuzaine, O. Bruno, and F. Reitich. On the O(1) solution of multiple-scattering problems. *IEEE Trans. Magn.*, 41(5):1488–1491, May 2005. 11th IEEE Biennial Conference on Electromagnetic Field Computation, Seoul, South Korea, June 06-09, 2004.

[29] L. Greengard and V. Rokhlin. A fast algorithm for particle simulations. *J. Comput. Phys.*, 73(2):325–348, 1987.

[30] M.J. Grote and C. Kirsch. Dirichlet-to-Neumann boundary conditions for multiple scattering problems. *J. Comput. Phys.*, 201(2):630 – 650, 2004.

[31] R.F. Harrington and J.R. Mautz. H-field, E-field and combined field solution for conducting bodies of revolution. *Archiv Elektronik und Uebertragungstechnik*, 4(32):157–164, 1978.

[32] C. Hazard and K. Ramdani. Selective acoustic focusing using time-harmonic reversal mirrors. *SIAM J. Appl. Math.*, 64(3):1057–1076, 2004.

[33] P. Hewageegana and V. Apalkov. Second harmonic generation in disordered media: Random resonators. *Physical Review B*, 77(7), 2008.

[34] Z. Hu and Y.Y. Lu. Compact wavelength demultiplexer via photonic crystal multimode resonators. *J. Opt. Soc. Am. B*, 31(10):2330–2333, Oct 2014.

[35] R.D. Meade J.D. Joannopoulos and J.N. Winn. *Photonic Crystals: Molding the Flow of Light.* Princeton University Press, 1995.

[36] A.A. Kharlamov and P. Filip. Generalisation of the method of images for the calculation of inviscid potential flow past several arbitrarily moving parallel circular cylinders. *Journal of Engineering Mathematics*, 77(1), 2012.

[37] P. A. Martin. *Multiple Scattering. Interaction of Time-Harmonic Waves with N Obstacles*, volume 107 of *Encyclopedia of Mathematics and its Applications*. Cambridge University Press, Cambridge, 2006.

[38] T.D. Mast, A.I. Nachman, and R.C. Waag. Focusing and imaging using the eigenfunctions of the scattering operator. *J. Acoust. Soc. Am.*, 102:715–725, 1997.

[39] H. Mertens, A. F. Koenderink, and A. Polman. Plasmon-enhanced luminescence near noble-metal nanospheres: Comparison of exact theory and an improved Gersten and Nitzan model. *Physical Review B*, 76(11), 2007.

[40] D.M. Natarov, V.O. Byelobrov, R. Sauleau, T.M. Benson, and A.I. Nosich. Periodicity-induced effects in the scattering and absorption of light by infinite and finite gratings of circular silver nanowires. *Optics Express*, 19(22176-22190), 2011.

[41] J.-C. Nédélec. *Acoustic and Electromagnetic Equations. Integral Representations for Harmonic Problems*, volume 144 of *Applied Mathematical Sciences*. Springer-Verlag, New York, 2001.

[42] O.K. Pashaev and O. Yilmaz. Power-series solution for the two-dimensional inviscid flow with a vortex and multiple cylinders. *Journal of Engineering Mathematics*, 65(2), 2009.

[43] C. Prada. The D.O.R.T. method. *J. Acoust. Soc. Am.*, 101(5):3090–3090, 1997.

[44] Y. Saad. *Iterative Methods for Sparse Linear Systems*. PWS Publishing Company Boston, 1996.

[45] S. Sauter and C. Schwab. *Boundary Element Methods*. Springer Science and Business Media, 2010.

[46] R. Savo, M. Burresi, T. Svensson, K. Vynck, and D.S. Wiersma. Walk dimension for light in complex disordered media. *Phys. Rev. A*, 90:023839, Aug 2014.

[47] B. Thierry. *Analyse et Simulations Numériques du Retournement Temporel et de la Diffraction Multiple*. Nancy University, Thèse de Doctorat, 2011.

[48] B. Thierry. A remark on the single scattering preconditioner applied to boundary integral equations. *Journal of Mathematical Analysis and Applications*, 413(1):212 – 228, 2014.

[49] J.-L. Thomas, F. Wu, and M. Fink. Time reversal focusing applied to lithotripsy. *Ultrasonic Imaging*, 18(2):106–121, 1996.

[50] L. Tsang, J.A. Kong, K.H. Ding, and C.O. Ao. *Scattering of Electromagnetic Waves, Numerical Simulation*. Wiley Series in Remote Sensing. J.A. Kong, Series Editor, 2001.

[51] S. Tulu and O. Yilmaz. Motion of vortices outside a cylinder. *Chaos*, 20(4), 2010.

[52] B. Van Genechten, B. Bergen, D. Vandepitte, and W. Desmet. A Trefftz-based numerical modelling framework for Helmholtz problems with complex multiple-scatterer configurations. *J. Comput. Phys.*, 229(6623-6643), 2010.

[53] D.S. Wiersma. Disordered photonics. *Nature Photonics*, 7:188–196, Feb 2013.